The International Journal of Advanced Manufacturing Technology (2019) 103:2235–2256
https://doi.org/10.1007/s00170-019-03421-x

ORIGINAL ARTICLE

Analytical and experimental investigation of the dynamic behavior of a revolute-prismatic manipulator with N flexible links and hubs

M. H. Korayem [1] · S. F. Dehkordi [1] · M. Mojarradi [1] · P. Monfared [1]

Received: 31 July 2018 / Accepted: 4 February 2019 / Published online: 17 April 2019

Abstract

In this paper, the dynamic model and vibration analysis of a flexible manipulator composed of N elastic links and robot actuators for which structural vibration is considered are investigated. In view of the concurrent linear and rotary motions of the link caused by revolute-prismatic joints, the interaction of joint's structural vibration and link fluctuation is taken as an effective model parameter. Utilization of prismatic joint with hub in the manipulator's structure in question, its significant length and low weight result in the operation of hub akin to a flexible link attached to revolute joint. To model the expressed hub oscillation with respect to the link, the assumed modes method and mode shapes of Euler-Bernoulli beam with independent generalized modal coordinate with respect to the link are employed. Noting the complexity of the present model relative to studied flexible manipulators, the recursive Gibbs-Appell formulation is used to derive the motion equations. Therefore, the dynamic equations of hub are of time-independent form, while these equations are obtained as time-variable for links. Although the obtained equations are simultaneously solved in the coupled form, the derived equations for a single-link flexible manipulator are simulated in three cases of (1) rigid hub, (2) elastic hub, and (3) elastic hub and flexible joints. The simulation results are compared with a similar experimental setup, indicating that the flexible manipulator model with elastic link, hub, and joints yields satisfactory results with an error of less than 1 mm and 1° in the longitudinal and rotational motions, respectively. Moreover, the results of lateral vibration show good accuracy, with the endpoint of the robot having perfect precision with just 1% tolerance.

Keywords Flexible link · Revolute-prismatic joints · Recursive Gibbs-Appell formulation · Experimental flexible manipulator

1 Introduction

Utilization of flexible link manipulators (FLM) has been rising recently due to their wide range of applications in industry, medicine, aerospace, instrumentation, satellites, and industrial automation [1]. Such manipulators are replacing rigid links with larger dimensions and more weight in various industries [2]. To facilitate the utilization process, manipulators with revolute joints along with time-invariable dynamic equations are used. Although this may simplify their employment, the robot accuracy and performance are limited in some cases [3]. As a result, utilizing mechanisms with higher accuracy and larger accessibility has gained attention despite structural complexities. Among such mechanisms, one can mention the prismatic joints by which linear motion with proper precision is achievable. The mere use of such joints results in a more complicated structure of manipulator, thus a more difficult modeling. When using flexible links along with prismatic joints, a different approach for system modeling is required depending on whether the prismatic joints have telescopic operation while prismatic joints have sleeves or are considered simple elements without a hub. In both cases and compared with revolute joints, however, the system dynamic equations become time-variable due to the linear motion and the change in the length of robot link. On the other hand, using a hub in prismatic joint structure and the change in the link length makes it possible to benefit from long links in different working situations and path generation in the existence of fixed or mobile obstacles. Although this may result in a simpler and more accurate displacement of the robot gripper, the change in the effective length causes variation in its vibration

Electronic supplementary material The online version of this article (https://doi.org/10.1007/s00170-019-03421-x) contains supplementary material, which is available to authorized users.

✉ M. H. Korayem
hkorayem@iust.ac.ir

[1] Robotics Research Laboratory, Center of Excellence in Experimental Solid Mechanics and Dynamics, School of Mechanical Engineering, Iran University of Science and Technology, Tehran, Iran

amplitude. As the motion is merely linear, its impact on the system dynamic behavior becomes noticeable for large values of length. Utilizing solely prismatic joints limits the gripper motion to a one-dimensional (1D) case. Nevertheless, simultaneous employment of revolute and prismatic joints in robotic manipulators for each link at the same time offers the capabilities of both revolute and prismatic joints to the user. Therefore, the vibration amplitude of flexible link motion depends on the lateral bending caused by both rotational and linear motions.

Different mechanisms exist for generating linear motion, among which, hydraulic jacks, rack and pinion, linear electric pumps, and linear guides can be mentioned. Rack and pinion can be used to generate linear motion when the backlash and friction in joints are not important. Linear electric pumps have been employed when a robot is utilized in a specific motion range for performing tasks in consecutive time steps while its trajectory and time is constant, and one may use this actuator as a prismatic joint. The linear guide is of central attention for precise applications due to the use of ball screws and their motion accuracy which is a function of pitch and electric motor exactness. Flexible systems are designed such that they can offer low weight and benefit from motors with less power compared with rigid systems. In mechanisms that create linear motion such as linear guides, the mentioned issue brings about structural vibrations, which, in conjunction with motor dynamics, affects the robot gripper vibration and link elasticity during motion. Although the dynamics of electric motors and joints in FLM with revolute joints has been investigated, no attention has been paid to the effect of structural vibrations due to the dynamic structure of joints. This topic is of great importance in manipulators with prismatic and revolute-prismatic (R-P) joints.

The link vibration is modeled with regard to the material, dimensions, and type of application. In the assumed modes method (AMM), the elastic deformations are obtained in a local form based on the estimated assumed mode shapes by considering the boundary conditions and application type of the link. It should be noted that the assumed mode shapes of the link are influenced by various parameters such as moment of inertia, joints' flexibility, concentrated mass, and other linear and nonlinear phenomena [4]. Accordingly, the flexibility and structural vibration of the joint should be considered in the calculations as two prominent factors. A number of approaches exist for modeling the structural vibration in different joint types [5]. Regarding the joint type, the amplitude of structural vibration in prismatic joints is higher than that in other joints. For instance, the methods used in hydraulic cranes [6] and telescopic joints [7] for modeling the structural vibration can be mentioned. AMM is also used for this purpose. Accordingly, the generalized modal coordinates are separated so as to estimate the vibratory characteristics of link and joint. At the same time, however, the interaction of the vibratory motion of link and joint is distinguished by considering the resultant of the elastic deformation of link and joint in order to model the dynamical behavior of flexible link.

In view of the described complexities, employing a modeling approach that results in an optimized derivation algorithm for motion equations in terms of calculation complexity is important. Therefore, by comparing the computational complexity of dynamic formulations for deriving the motion equations [8], the extended recursive Gibbs-Appell (G-A) formulation is preferred over Euler-Lagrange (E-L) and Hamilton and Newton-Euler (N-E) equations as well as Kane's formulation. Book [9] derived the motion equations of a manipulator with N flexible links aided by the recursive E-L equations. 4×4 matrices were used to describe the robot motion, and the computational complexity of the presented formulation was also evaluated. Korayem et al. [10] extended this method by considering the Timoshenko beam theory, 3×3 transformation matrices, and comparing with an experimental system using the recursive G-A formulation. Despite the discussion on the N-link model of flexible manipulators with revolute joints, there exist numerous researches having derived the equations only for special cases while considering effective external parameters to increase modeling accuracy [11]. Flexibility [12], backlash [13] and friction [14] of joints, structural damping of links [15], and structural vibration of joints [16] are among these parameters. In most of these cases, the E-L formulation is used to derive the equations, although the closed form of the N-E formulation [17] as well as the extended recursive G-A formulation [18] has also been considered.

Theodore et al. [19] derived the motion equations of a FLM with prismatic joints using the E-L equations. Precise and rapid motion of these joints has led to their utilization in different structures with rigid or flexible links, as studied by Yüksel and Gürgöze [20] and Sharifnia [21]. Extension of prismatic joints employment in conjunction with revolute joints has been an interesting subject for many researchers [22–25], although most conducted studies are based on manipulators with only one or two flexible links. Korayem et al. [26] investigated such joints in manipulators with N flexible links. In all of the presented studies thus far, the effect of prismatic joint's hub has been neglected by considering it to be an element with no mass in the equations. This is in spite of the fact that in real-life systems, it acts as a link with revolute joint. In addition, when low-elasticity materials are used in the construction of prismatic joints, the rigidity assumption is not valid and the motion vibrations caused by its operation can have certain effects on other components, as previously illustrated [7]. To consider structural vibration, the magnitude of hub vibration is locally calculated aided by the beam mode shapes with similar boundary conditions, dimensions, and geometry [27, 28]. To evaluate the obtained dynamic formulation, experimental systems with similar working conditions are utilized. Most existing experimental setups are constructed as dual-link systems with revolute joints and flexible links, as

examined by Vakil et al. [29], Korayem et al. [10], and Pradhan and Subudhi [30]. Regarding prismatic joints, however, few robots have been built, mostly with industrial applications. The studies by Ju et al. [31], Zhang et al. [32], and Mastory and Chalhoub [33] have dealt with such robots.

In this paper, the dynamic model of an N-link manipulator with flexible revolute-prismatic joints, link, and structure is obtained. To derive the system motion equations, the recursive G-A formulation along with the AMM is employed. Compared with other existing mechanisms, the R-P joints are affected by the motion of constituent components in view of the concurrent rotary and linear motions of the flexible link. Accordingly, the impact of mass and elasticity of the prismatic joint's hub should be duly considered in the equations. Therefore, the main contribution of this paper includes modeling the joints' structural vibration using AMM, illustration of interaction between joints and links' fluctuations, and deriving the FLM motion equations with both structural and links' flexibility considered. A simulation is carried out for a single-link manipulator in both cases of rigid and elastic hub along with the effect of joints' flexibility. To validate the findings, the results are compared with the data obtained from testing the similar experimental setup in the robotic laboratory of Iran University of Science and Technology (IUST). In Section 2, the specifications of the experimental setup are presented. Section 3 deals with the derivation method of dynamic equations. A mathematical simulation is developed in Section 4 and the accuracy of outputs are evaluated. In the end, the obtained results are analyzed.

2 Experimental setup of FLM with R-P joints

According to Fig. 1, the experimental setup is composed of a single-link manipulator with R-P joints on a fixed platform. The mechanical properties of this robot are presented in Table 1.

The exploded view of the designed structure in SolidWorks is shown in Fig. 2 and the components are listed in Table 2. The rotational motion in the built robot is directly transferred to the axis of the revolute joint by the AC servo-motor without using the gearbox. To this end, a flange (part no. 3 in Fig. 2) is used. In practice, the prismatic joint's hub and the link apply the bending moment to the revolute joint's motor axis. To prevent the direct pressure of bending load, a bearing is also implemented to connect the coupling and motor axis. The stiffness coefficient for this part is considered the joint's flexibility in the dynamic model in the following section. For this reason, the performance of servo-motor and bearing is treated as a rotational spring with constant coefficient. This spring connects the prismatic joint's hub and motor axis in the model derivation assumption. To obtain this coefficient, it is necessary to perform rotary motion without any changes in axial motion by importing a specific range of torques to the revolute joint. The concluded flexibility of revolute joint is exhibited in Table 3.

The specifications of the utilized motor set including motor, driver, encoder, and mechanical brake in the revolute joint are presented in Table 1. This motor can be adjusted in three operation modes: (1) torque, (2) velocity, and (3) position. The torque mode will be used for forward dynamic simulation. The encoder is capable of measuring 2500 pulses per revolution, and changing the method of measuring passes can increase its accuracy up to 10,000 pulses per revolution. Consequently, its measurement accuracy is about 0.036°. To generate linear motion in this robot, the mechanism of linear guide, composed of ball screw, bearings, ball screw pitch, guide beam, aluminum profile, and wagon, is utilized. The system lead after one turn of ball screw is 2.5 mm with a linear motion accuracy of about 0.1 mm. The motion of prismatic

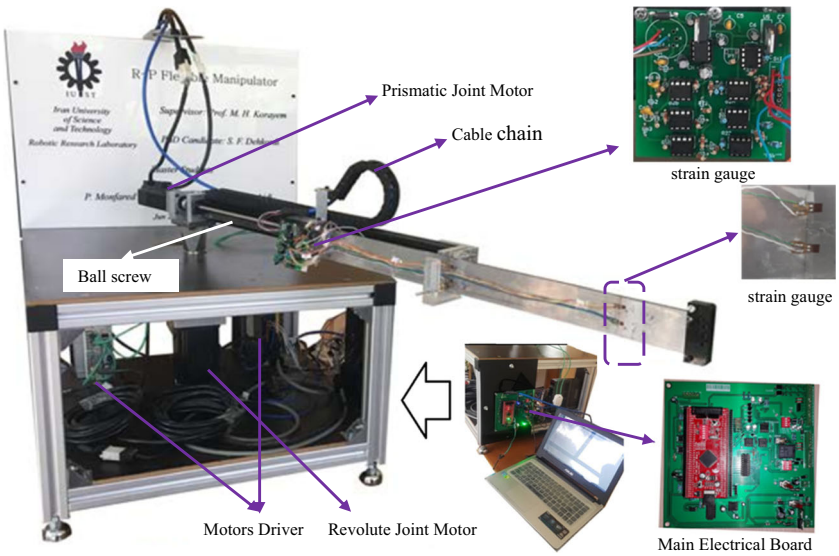

Fig. 1 The IUST experimental setup with single flexible link and R-P joint

Table 1 Mechanical properties of flexible manipulator with R-P joints

Parameters	Description	Specifications
Revolute joint's motor	Leadshine AC servo 750 W with break	2.4 N·m-rated torque 3000 RPM-rated speed 4.5 A-rated current
Prismatic joint's motor	LS AC servo 100 W without break	0.32 N·m-rated torque 3000 RPM-rated speed
Ball screw	TBI motion	Lead = 2.5 mm

joint is realized with the aid of an AC motor. The electric motor consists of motor, driver, and encoder. In view of system settings and nominal RPM of the electric motor of this joint, its maximum linear velocity is equal to 65 mm/s.

The flexible link dimensions and specifications are listed in Table 3. To install it on the wagon, a connector is utilized (part no. 17 in Fig. 2). This connector provides the minimum required space for link oscillation during the motion as well as preventing the strain gauge's wires from damage.

To measure the elastic deformation of link, 350-Ω Joksing strain gauges are implemented. When strain gauges are used to record link oscillation, different strategies exist to attach them on link such as Quarter Bridge, Half Bridge, and Full Bridge. The number of strain gauges needed to evaluate link deformation, sensitivity to environmental conditions, deformations direction evaluated, and measuring accuracy is different in each one. By considering these features, the Full Bridge approach has been used in this study where strain gauges are installed on 3 points of the link in pairs. The four installed strain gauges form a Wheatstone bridge while it minimize temperature effects and being sensitive to bending strain. It should be mentioned that due to the link size, the fluctuations in other side can be neglected. In view of better operation of strain gauges, the strain gauge circuit is located on the wagon of prismatic joint in the nearest possible distance. To calculate the elastic deformation generated in the link during motion, the approach described in Ref. [8] is utilized: in view of boundary condition and placement of strain gauges on the link, a relation is fitted using its elastic deformation. Using the obtained data, the elastic deformation is calculated at each instant of time. Unlike Ref. [8], to obtain the link elastic deformation of this robot, the effective length of robot link varies with time. Consequently, the boundary conditions and obtained values at any moment should be recalculated. The computation algorithm is presented in Appendix (C).

When deriving the motion equations, it is assumed that the link can fluctuate outside the hub due to its elasticity. However, when the link reciprocates through the prismatic joint's hub, the part of the link placed in the sleeves does not have oscillations by itself because of the limited range of vibration in the joint's hub. It is emphasized that the link and its hub have swing motion due to hub elasticity. Having this considered, part no. 13 is used in Fig. 2, constraining the link motion by two rollers and providing cantilevered boundary conditions. According to Fig. 3, the main electronic circuit of robot has the mission of signal processing as well as sending and receiving the data. The constituent components are as follows: digital to analog converters (DAC), analog to digital converters (ADC), data acquisition system of encoders, brake command of rotary motor, and opto-couplers. Its central processing unit (LPC 1768-32bit ARM Cortex-M3) is among powerful micro-controllers which offers special features to the designers due to its DACs.

3 Dynamic modeling of N-link flexible manipulator with R-P joints and structural vibration

To model FLM in question, each arm, which is composed of (1) a link with rotational and reciprocating motion and (2) a hub having rotary motion and structural vibration, is distinctly

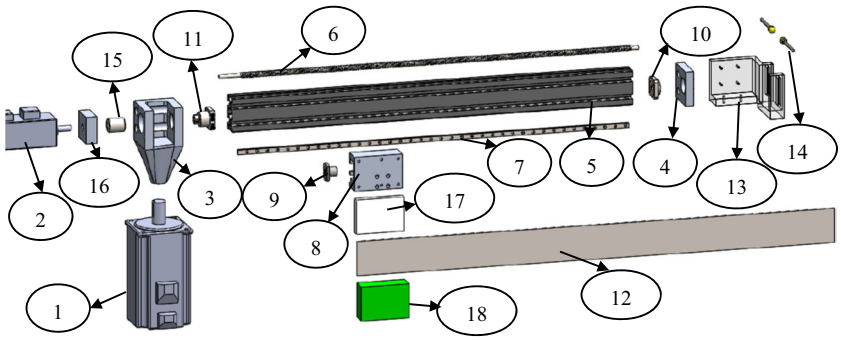

Fig. 2 The exploded view of IUST single flexible link and R-P joint

Table 2 Different parts of flexible manipulator with R-P joints

Number	Description	Number	Description	Number	Description
1	750-W motor	7	Linear guide	13	Hub constrainer
2	100-W motor	8	Wagon	14	Damper
3	First cap	9	Ball screw nut	15	Coupling
4	End cap	10	End ball bearing	16	Motor's spacer
5	Aluminum profile	11	First ball bearing	17	Elastic beam's spacer
6	Ball screw	12	Steel beam	18	Strain gauge's PCB board

modeled. In this case, the effect of link and hub vibrations is applied by considering different mode shapes and generalized modal coordinates with AMM approach. In view of the oscillatory interaction of link and hub, the effect of hub vibration on the link should also be considered. Accordingly, as shown in Fig. 3, the system kinematic vectors are first obtained, then the dynamic equations of flexible hub and link are separately calculated. In the end, the general robot motion equations are obtained. The effect of flexible hub in the model is taken to be analogous to a flexible link in a manipulator exclusively having revolute joints.

3.1 FLM kinematic modeling

According to Fig. 4, the differential elements Q and $Q^{'}$ are arbitrarily selected on the ith link and joint's hub. The position vectors of these two elements relative to the origin of the coordinate system attached to the ith link (O_i) are, respectively, shown by ${}^{i}r_{Q/O_i}$ and ${}^{i}r_{Q^{'}/O_i}$. The differential element Q is affected by two rotational and linear rigid-body motions along with two vibration modes caused by the elasticity of link and hub.

Table 3 Physical parameters of flexible manipulator with R-P joints

Parameter		Description	Value
Link	L_1	Length	0.7m
	W_1	Width	0.05m
	T_1	Thickness	0.002m
	E_1	Elasticity	1.9×10^{11} N×m^{-2}
	K_v	Kelvin-Voigt coefficient	3000kg · s · m^{-1}
	γ	Air damping coefficient	1.0kg · s · m^{-1}
	μ_1	Mass per unit length	0.785kg · m^{-1}
Hub	$L_1^{'}$	Length	0.7m
	$W_1^{'}$	Width	0.05m
	$T_1^{'}$	Thickness	0.052m
	$E_1^{'}$	Elasticity	1.3×10^{11} N · m^{-2}
	$\mu_1^{'}$	Mass per unit length	2.1424kg · m^{-1}
g		Gravity acceleration	10m · s^{-2}
K_R^m		Revolute joint flexibility	1000 N · rad^{-1}
I_R^m		Revolute joint inertia	0.05m^3

The differential element Q is merely affected by the rigid-body motion due to rotation and the vibration mode caused by the elasticity of link and hub. Hence, the relative position vectors of these two elements are defined as:

$$ {}^{i}r_{Q/O_i} = \begin{Bmatrix} \eta^{i}x_i + \{u_i(\eta)\ v_i(\eta)\ w_i(\eta)\}^T + \left\{u^{'}\left(L_i^{'}\right)\ v_i^{'}\left(L_i^{'}\right)\ w_i^{'}\left(L_i^{'}\right)\right\}^T & for\ \eta \geq L_i^{'} \\ \eta^{i}x_i + \left\{u_i^{'}(\eta)\ v_i^{'}(\eta)\ w_i^{'}(\eta)\right\}^T & for\ \eta \geq L_i^{'} \end{Bmatrix} \quad (1) $$

$$ {}^{i}r_{Q^{'}/O_i} = \eta^{i}x_i + \left\{u^{'}(\eta)\ v_i^{'}(\eta)\ w_i^{'}(\eta)\right\}^T \quad (2) $$

where η is the relative position vector of the mentioned elements in the static form without any deformation; $L^{'}$ is the hub length; L is the link length; u, v, and w are the elastic deformation components of link; and the same values with the prime sign signify the deformation components of elastic hub. To calculate the elastic deformations, the AMM is employed. Using the developed modal expansion, the amount of link vibration is evaluated based on the multiplication of assumed mode shape according to the system conditions, the beam geometry by which the link or hub behavior is estimated $\left(r_{ij}(\eta,t), r_{ij}^{'}(\eta)\right)$, and the generalized modal coordinates $\left(\delta_{ij}(t), \delta_{ij}^{'}(t)\right)$. Therefore, $r_{ij}, r_{ij}^{'}$ are merely functions of the differential element position. However, the vector of link mode shapes ($r_{ij}(\eta,t)$) changes with time as a result of its longitudinal motion in the direction of hub and the change in its effective length. Euler-Bernoulli mode shapes of a clamped-free beam are exploited:

$$ \begin{aligned} \{u_i \quad v_i \quad w_i\}^T &= \sum_{j=1}^{m_i} \delta_{ij}(t) r_{ij}(\eta,t) \\ \{u_i^{'} \quad v_i^{'} \quad w_i^{'}\}^T &= \sum_{j=1}^{m_i^{'}} \delta_{ij}^{'}(t) r_{ij}^{'}(\eta) \end{aligned} \quad (3) $$

where m_i and $m_i^{'}$ denote the number of these assumed mode shapes. Likewise, the angular deformations of link and hub are found by considering the generalized modal coordinates similar to what is presented in Eq. (3) in conjunction with the mode shapes $\theta_{ij}(\eta,t), \theta_{ij}^{'}(\eta)$.

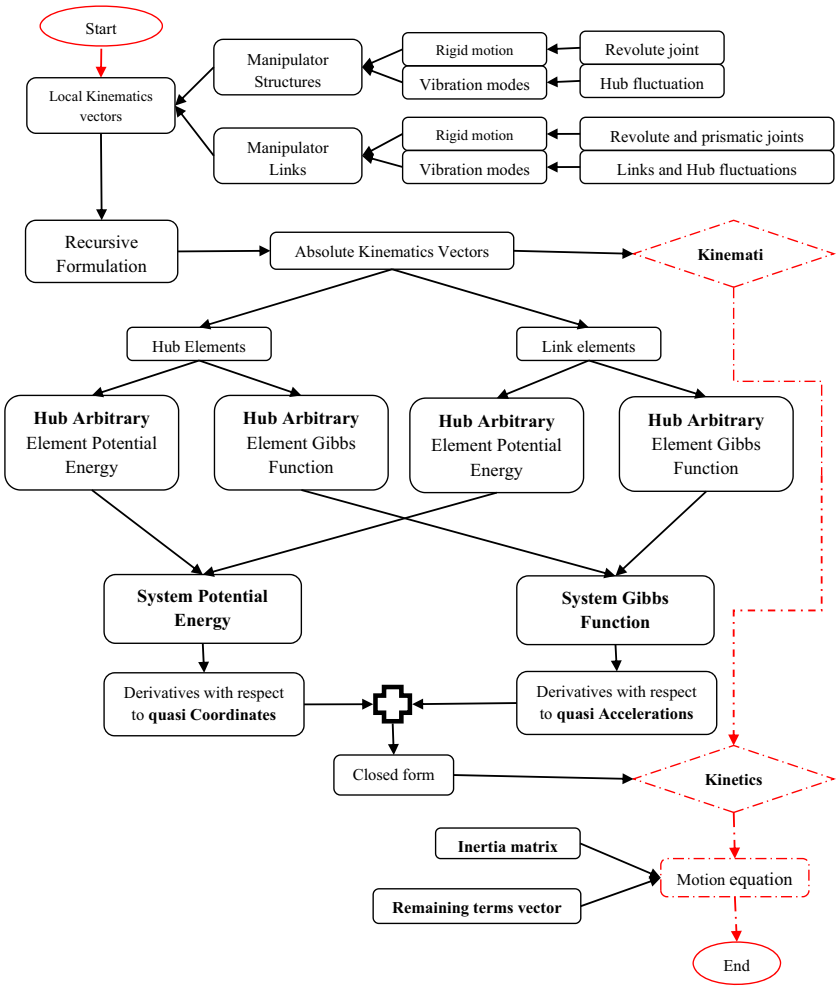

Fig. 3 Flowchart of motion equation derivation by recursive G-A formulation

$$\begin{aligned}\left\{\theta'_{xi}\quad\theta'_{yi}\quad\theta'_{zi}\right\}^T &= \sum_{j=1}^{m'_i}\delta'_{ij}(t)\theta'_{ij}(\eta) \qquad for\ Hub\\ \left\{\theta_{xi}\quad\theta_{yi}\quad\theta_{zi}\right\}^T &= \sum_{j=1}^{m_i}\delta_{ij}(t)\theta_{ij}(\eta,t)\\ &\quad+\sum_{j=1}^{m'_i}\delta'_{ij}(t)\theta'_{ij}\left(L'_i\right)+for\ Link\end{aligned} \tag{4}$$

The vectors obtained through Eqs. (1) and (2) are found in the local coordinates. To evaluate the system energy, one must define the kinematic values utilized in the reference coordinate system $X_0Y_0Z_0$. Consequently, to reduce the complexity of calculations, recursive approaches are employed and the vectors of linear and angular acceleration of both elements are obtained relative to this system.

$$\begin{aligned}{}^{i}\ddot{\mathbf{r}}_Q &= {}^{i}\ddot{\mathbf{r}}_{O_i}+{}^{i}\ddot{\mathbf{r}}_{Q/O_i}+2\left({}^{i}\boldsymbol{\omega}_i\times{}^{i}\dot{\mathbf{r}}_{Q/O_i}\right)\\ &+\left({}^{i}\dot{\boldsymbol{\omega}}_i\times{}^{i}\mathbf{r}_{Q/O_i}\right)+\left\{{}^{i}\boldsymbol{\omega}_i\times\left({}^{i}\boldsymbol{\omega}_i\times{}^{i}\mathbf{r}_{Q/O_i}\right)\right\}{}^{i}\ddot{\mathbf{r}}Q'\\ &={}^{i}\ddot{\mathbf{r}}_{O_i}+{}^{i}\ddot{\mathbf{r}}_{Q'/O_i}+2\left({}^{i}\boldsymbol{\omega}_i\times{}^{i}\dot{\mathbf{r}}_{Q'/O_i}\right)+\left({}^{i}\dot{\boldsymbol{\omega}}_i\times{}^{i}\mathbf{r}_{Q'/O_i}\right)\\ &+\left\{{}^{i}\boldsymbol{\omega}_i\times\left({}^{i}\boldsymbol{\omega}_i\times{}^{i}\mathbf{r}_{Q'/O_i}\right)\right\}\end{aligned} \tag{5}$$

$$\begin{aligned}{}^{i}\dot{\omega}_i &= {}^{i}R_{i-1}\left({}^{\mathrm{i-1}}\dot{\omega}_{i-1}+{}^{\mathrm{i-1}}\ddot{\theta}_{i-1}+{}^{\mathrm{i-1}}\omega_{i-1}\times{}^{\mathrm{i-1}}\dot{\theta}_{i-1}\right)\\ &+{}^{i}R_{i-1}\left({}^{\mathrm{i-1}}\omega_{i-1}+{}^{\mathrm{i-1}}\dot{\theta}_{i-1}\right)\times{}^{i}z_i\dot{q}_i+{}^{i}z_i\ddot{q}_i\end{aligned} \tag{6}$$

where ${}^{i}\ddot{\mathbf{r}}$ is the acceleration of the origin of coordinate system attached to the i 'th link. In addition, ${}^{i}\ddot{\mathbf{r}}_{Q/O_i}$ and ${}^{i}\dot{\mathbf{r}}_{Q'/O_i}$ are the derivatives of Eq. (2) with respect to time, ${}^{\mathrm{i}}\mathbf{R}_{\mathrm{i}-1}$ is the rotational matrix between the origin of coordinate system attached to the i 'th and $(i-1)$ 'th link (${}^{j}\mathbf{R}_i={}^{j}\mathbf{R}_{i-1}\mathbf{E}_{i-1}\mathbf{A}_i$), and ${}^{\mathrm{i-1}}\dot{\boldsymbol{\theta}}_{\mathrm{i-1}}$ and ${}^{\mathrm{i-1}}\ddot{\boldsymbol{\theta}}_{\mathrm{i-1}}$ are the time derivatives of Eq. (4). In view of the amount of computations, the vector ${}^{i}\ddot{\mathbf{r}}$ is found by recursive means in terms of previous arms:

$$\begin{aligned}{}^{i}\mathbf{r}_{O_i} &= {}^{\mathrm{i-1}}\ddot{\mathbf{r}}_{O_{i-1}}+{}^{\mathrm{i-1}}\ddot{\mathbf{r}}_{O_i/O_{i-1}}+2\left({}^{\mathrm{i-1}}\boldsymbol{\omega}_{i-1}\times{}^{\mathrm{i-1}}\dot{\mathbf{r}}_{O_i/O_{i-1}}\right)\\ &+\left({}^{\mathrm{i-1}}\dot{\boldsymbol{\omega}}_{i-1}\times{}^{\mathrm{i-1}}\mathbf{r}_{O_i/O_{i-1}}\right)\\ &+\left\{{}^{\mathrm{i-1}}\boldsymbol{\omega}_{i-1}\times\left({}^{\mathrm{i-1}}\boldsymbol{\omega}_{i-1}\times{}^{\mathrm{i-1}}\mathbf{r}_{O_i/O_{i-1}}\right)\right\}\end{aligned} \tag{7}$$

where ${}^{\mathrm{i-1}}\mathbf{r}_{O_i/O_{i-1}}$ is the position vector of the origin of coordinate system attached to the i 'th link relative to the origin of

coordinate system attached to the (i-1) i '*th* link and described in the (i-1) '*th* coordinate system:

$$
\begin{aligned}
{}^{i-1}r_{O_i/O_{i-1}} &= \left(L'_{i-1} + l_{i-1}\right)^{i-1}x_{i-1} \\
&+ \{u_i(l_{i-1})\ v_i(l_{i-1})\ w_i(l_{i-1})\}^T \\
&+ \left\{u'\left(L'_{i-1}\right)\ v'_i\left(L'_{i-1}\right)\ w'_i\left(l'_{i-1}\right)\right\}^T
\end{aligned} \tag{8}
$$

where l_{i-1} is the proportion of the link length outside of the (i−1)th link at each instant of time.

3.2 FLM dynamic modeling

Obtaining the dynamic model of N-link flexible manipulator in view of the elasticity of the hub of prismatic joints and link is of interest in this section. A flexible hub is taken as a flexible link with revolute joint, while the link motion is under the influence of rotational and linear motions of joints and the interaction of two vibration modes of link and hub. To this end, the dynamic model of hub and links is independently obtained. This is followed by considering each of them in the formation of system inertia matrix and the vector of remaining forces.

3.2.1 Dynamic modeling of the elastic hub of prismatic joint

In order to calculate the motion equations in the recursive G-A formulation (Fig. 3), the values of acceleration and potential energy of hub are evaluated. Then, by differentiating with respect to the system generalized quasi-accelerations and summing them, the final form of equations are found. For the flexible hub, the state variables are $\mathbf{q}_i = (q_1, q_2, \ldots, q_n)^{\mathrm{T}}$ and $\boldsymbol{\delta}'_{ij} = \left(\delta'_{11}, \ldots, \delta'_{1m(1)}, \ldots, \delta'_{n1}, \ldots, \delta'_{nm(n)}\right)$. The number of degrees of freedom in general case is equal to $n + \sum_{i=1}^{n} m'(i)$.

- Gibbs function of elastic hub

$$
\begin{aligned}
S_H &= \sum_{i=1}^{n}\int_0^{L'_i} ds_{H_i} \\
S_H &= \sum_{i=1}^{n}\left(\frac{1}{2}B'_{0i}\,{}^{i}\ddot{r}_{O_i}^{T} \times {}^{i}\ddot{r}_{O_i}\right) + \left({}^{i}\ddot{r}_{O_i}^{T} \times {}^{i}B'_{1i}\right) \\
&-2\left({}^{i}\ddot{r}_{O_i}^{T} \times B'_{2i}\,{}^{i}\omega_i\right) - \left({}^{i}\ddot{r}_{O_i}^{T} \times B'_{3i}\,{}^{i}\dot{\omega}_i\right) - \left({}^{i}\ddot{r}_{O_i}^{T} \times {}^{i}\tilde{\omega}_i B'_{3i}\,{}^{i}\omega_i\right) \\
&+\frac{1}{2}B'_{4i} - 2\left({}^{i}\omega_i^{T} \times {}^{i}B'_{5i}\right) + \left({}^{i}\dot{\omega}_i^{T} \times {}^{i}B'_{6i}\right) - \left({}^{i}\omega_i^{T} \times {}^{i}B'_{7i}\,{}^{i}\omega_i\right) \\
&+2\left({}^{i}\dot{\omega}_i^{T} \times B'_{8i}\,{}^{i}\omega_i\right) + \frac{1}{2}\left({}^{i}\dot{\omega}_i^{T} \times B'_{9i}\,{}^{i}\dot{\omega}_i\right) \\
&+\left({}^{i}\dot{\omega}_i^{T} \times {}^{i}\tilde{\omega}_i B'_{9i}\,{}^{i}\omega_i\right) + \textit{irrelevant terms}
\end{aligned} \tag{9}
$$

where ${}^{i}\tilde{\omega}_i$ is the skew-symmetric matrix related to the angular velocity of the i '*th* arm. The last terms are those that are not functions of the quasi-accelerations and are, therefore, neglected in the remainder of calculations. The terms shown by *irrelevant terms* indicate the parts of Gibbs function that do not depend on quasi-accelerations and should be omitted later when differentiating with respect to them. Therefore, they were collectively summarized in this term. By using these approaches, the computation process is reduced and the values of intermediate variables can be found similar to those presented in Ref. [34].

- Potential energy of elastic hub

The system potential energy due to the gravity enters the equations by considering the base acceleration ($^{0}\ddot{\vec{r}}_{O_0} = g\vec{Y}_0$) in the opposite direction. The potential energy due to the hub elasticity is considered:

$$
V_H = \frac{1}{2}\sum_{i=1}^{n}\sum_{j=1}^{m'_i}\sum_{k=1}^{m'_i}\delta'_{ij}(t)\delta'_{ik}(t)K'_{ijk} \tag{10}
$$

where

$$
K_{ijk} = \int_0^{L'_i}\left[\begin{array}{l}
\left(E'_i I'_{yi}\dfrac{\partial\theta'_{yij}}{\partial\eta}\dfrac{\partial\theta'_{yik}}{\partial\eta}\right) + \left(E'_i I'_{zi}\dfrac{\partial\theta'_{zij}}{\partial\eta}\dfrac{\partial\theta'_{zik}}{\partial\eta}\right) \\
+\left(E'_i A'_i\dfrac{\partial x'_{ij}}{\partial\eta}\dfrac{\partial x'_{ik}}{\partial\eta}\right) + \left(G'_i I'_{xi}\dfrac{\partial\theta x'_{xij}}{\partial\eta}\dfrac{\partial\theta'_{xik}}{\partial\eta}\right)
\end{array}\right] d\eta \tag{11}
$$

3.2.2 Dynamic modeling of flexible link

The state variables for the rigid-body motion of flexible link are $\mathbf{q} = (q_1, q_2, \ldots, q_n)^{\mathrm{T}}$ and $\boldsymbol{\eta} = (\eta_1, \eta_2, \ldots, \eta_n)^{\mathrm{T}}$. In addition, the system vibration modes are $\boldsymbol{\delta}_{ij} = (\delta_{11}, \ldots, \delta_{1m(1)}, \ldots, \delta_{n1}, \ldots, \delta_{nm(n)})$ and $\boldsymbol{\delta}'_{ij} = \left(\delta'_{11}, \ldots, \delta'_{1m(1)}, \ldots, \delta'_{n1}, \ldots, \delta'_{nm(n)}\right)$. The number of degrees of freedom in the general case is $2n + \sum_{i=1}^{n}\left(m'(i) + m(i)\right)$.

- Gibbs function of elastic link

$$
\begin{aligned}
S_L &= \sum_{i=1}^{n}\int_{l_i}^{L'_i+l_i} ds_{L_i} \\
S_L &= \sum_{i=1}^{n}\left(\frac{1}{2}B_{0i}\,{}^{i}\ddot{r}_{O_i}^{T} \times {}^{i}\ddot{r}_{O_i}\right) + \left({}^{i}\ddot{r}_{O_i}^{T} \times {}^{i}B_{li}\right) - 2\left({}^{i}\ddot{r}_{O_i}^{T} \times B_{2i}\,{}^{i}\omega_i\right) \\
&-\left({}^{i}\ddot{r}_{O_i}^{T} \times B_{3i}\,{}^{i}\dot{\omega}_i\right) - \left({}^{i}\ddot{r}_{O_i}^{T} \times {}^{i}\tilde{\omega}_i B_{3i}\,{}^{i}\omega_i\right) + \frac{1}{2}B_{4i} - 2\left({}^{i}\omega_i^{T} \times {}^{i}B_{5i}\right) \\
&+\left({}^{i}\dot{\omega}_i^{T} \times {}^{i}B_{6i}\right) - \left({}^{i}\omega_i^{T} \times B_{7i}\,{}^{i}\omega_i\right) + 2\left({}^{i}\dot{\omega}_i^{T} \times B_{8i}\,{}^{i}\omega_i\right) \\
&+\frac{1}{2}\left({}^{i}\dot{\omega}_i^{T} \times B_{9i}\,{}^{i}\dot{\omega}_i\right) + \left({}^{i}\dot{\omega}_i^{T} \times {}^{i}\tilde{\omega}_i B_{9i}\,{}^{i}\omega_i\right) + \textit{irrelevant terms}
\end{aligned} \tag{12}
$$

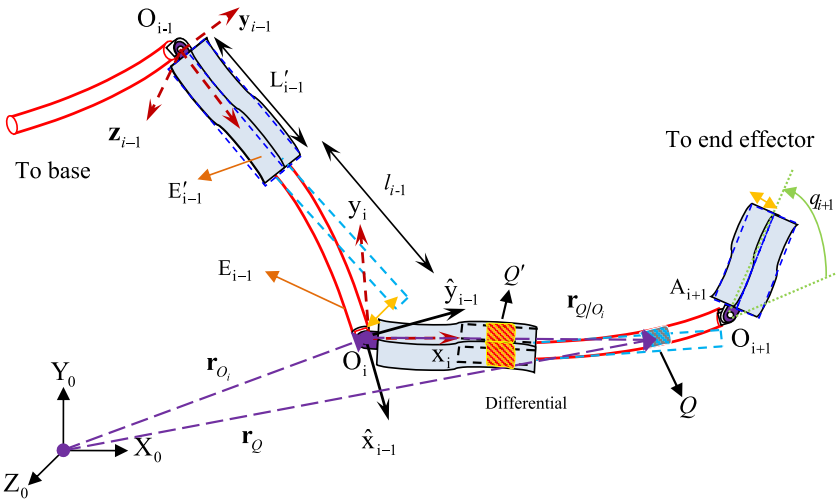

Fig. 4 N-link manipulator with flexible links and structures

Moreover, the values of intermediate variables **B** in this equation are as

$$B_{0i}=\int_{l_i}^{L_i+l_i}\mu_i(\eta)d\eta \qquad B_{0i}^{l}=\int_{L_i'}^{L_i+l_i}\mu_i(\eta)d\eta \quad {}^{i}B_{1i}+B_{0i}\ddot{\eta}_i{}^{i}x_i+\sum_{j=1}^{m(i)}\ddot{\delta}_{ij}C_{1ij}+B_{0i}^{l}\sum_{j=1}^{m'(i)}\ddot{\delta}_{ij}'r_{ij}'\left(L_i'\right)$$

$$B_{2i}=B_{0i}\dot{\eta}_i{}^{i}\tilde{x}_i+\sum_{j=1}^{m(i)}\dot{\delta}_{ij}\tilde{C}_{1ij}+B_{0i}^{1}\cdot\sum_{j=1}^{m'(i)}\dot{\delta}_{ij}'\tilde{r}_{ij}'\left(\mathrm{L}_i'\right) \qquad B_{3i}=C_{2i}+\sum_{j=1}^{m(i)}\delta_{ij}\tilde{C}_{1ij}+\sum_{j=1}^{m'(i)}\delta_{ij}'\tilde{r}_{ij}'\left(\mathrm{L}_i'\right)$$

$$B_{4i}=B_{0i}\ddot{\eta}_i^{2}+\sum_{j=1}^{m(i)}\ddot{\delta}_{ij}\left(2\ddot{\eta}_iC_{3ij}+\sum_{k=1}^{m(i)}\ddot{\delta}_{ik}C_{4ijk}\right)+B_{0i}^{l}\cdot\sum_{j=l}^{m'(i)}\ddot{\delta}_{ij}'\left(2\ddot{\eta}_i{}^{i}x_i^{T}r_{ij}'\left(L_i'\right)+\sum_{k=1}^{m(i)}\ddot{\delta}_{ik}'r_{ij}'{}^{T}\left(\mathrm{L}_i'\right)r_{ij}'\left(\mathrm{L}_i'\right)\right)$$

$$\begin{aligned}{}^{i}B_{5i}&=\sum_{j=1}^{m(i)}\left(\left(\dot{\delta}_{ij}\ddot{\eta}_i-\ddot{\delta}_{ij}\dot{\eta}_i\right)C_{5ij}+\sum_{k=1}^{m(i)}\ddot{\delta}_{ij}\dot{\delta}_{ik}C_{6ijk}\right)+B_{0i}^{l}\cdot\sum_{j=1}^{m'(i)}\left(\left(\dot{\delta}_{ij}'\ddot{\eta}_i-\ddot{\delta}_{ij}'\dot{\eta}_i\right)\cdot{}^{i}\tilde{x}_ir_{ij}'\left(L_i'\right)\right)+\sum_{j=1}^{m'(i)}\sum_{k=1}^{m(i)}\ddot{\delta}_{ij}\dot{\delta}_{ik}'\tilde{C}_{1ij}r_{ik}'\left(L_i'\right)\\&+\sum_{j=1}^{m'(i)}\left(\sum_{k=1}^{m(i)}\ddot{\delta}_{ij}'\dot{\delta}_{ik}r_{ik}'\left(L_i'\right)C_{1ik}+B_{0i}^{l}\cdot\sum_{j=1}^{m'(i)}\ddot{\delta}_{ij}'\dot{\delta}_{ik}'\left(\tilde{r}_{ij}'\left(\mathrm{L}_i'\right)r_{ik}'\left(\mathrm{L}_i'\right)\right)\right)\end{aligned}\qquad(12-\mathrm{A})$$

$${}^{i}B_{6i}=\sum_{j=1}^{m'(i)}\left(\ddot{\delta}_{ij}\alpha_{ij}-\ddot{\eta}_i\delta_{ij}C_{5ij}\right)+\sum_{j=1}^{m(i)}\left(\dot{\delta}_{ij}'\alpha_{ij}^{l}-B_{0i}^{l}\dot{\eta}_i\delta_{ij}'{}^{i}\tilde{x}_ir_{ij}'\left(L_i'\right)\right)\qquad B_{7i}=\sum_{j=1}^{m(i)}\left(\ddot{\eta}_i\left(\delta_{ij}C_{8ij}^{T}+C_{7i}\right)+\ddot{\delta}_{ij}\beta_{ij}\right)+\sum_{j=1}^{m'(i)}\left(\ddot{\eta}_i\left(\delta_{ij}'\tilde{\mathrm{r}}_{ij}'{}^{T}\left(\mathrm{L}_i'{}^{i}\mathbf{x}_i\right)+\ddot{\delta}_{ij}'\beta_{ij}^{l}\right)\right.$$

$$\begin{aligned}B_{8i}&=\sum_{j=1}^{m(i)}\left(\dot{\eta}_i\left(\delta_{ij}C_{8ij}^{T}+C_{7i}\right)+\dot{\delta}_{ij}\beta_{ij}\right)\\&+\sum_{j=1}^{m(i)}\left(\dot{\eta}_i\left(\delta_{ij}'\tilde{\mathrm{r}}_{ij}'{}^{T}\left(\mathrm{L}_i'{}^{i}\mathbf{x}_i\right)+\dot{\delta}_{ij}'\beta_{ij}^{l}\right)B_{9i}=C_{7i}'+\sum_{j=1}^{m(i)}\delta_{ij}\left(C_{8ij}'{}^{T}+\beta_{ij}\right)+\sum_{j=1}^{m'(i)}\delta_{ij}'\left(C_{2i}\tilde{\mathrm{r}}_{ij}'{}^{T}(\mathrm{L}_i')+\beta_{ij}^{l}\right)\right.\end{aligned}$$

The values of other intermediate variables in this equation can be found from the following equations:

$$C_{1ij}=\int_{L_i}^{L_i+l_i}\mu_ir_{ij}d\eta_i \qquad \tilde{C}_{1ij}=\int_{L_i}^{L_i+l_i}\mu_i\tilde{r}_{ij}d\eta_i \qquad C_{2i}=\int_{l_i}^{L_i+l_i}\mu_i\eta_i{}^{i}\tilde{x}d\eta_i$$

$$C_{3ij}=\int_{L_i}^{L_i+l_i}\mu_i\,{}^{i}x_i^{T}\cdot r_{ij}d\eta_i \qquad C_{4ijk}=\int_{L_i}^{L_i+l_i}\mu_i\,r_{ij}^{T}\cdot r_{ik}d\eta_i \qquad C_{5ij}=\int_{L_i}^{L_i+l_i}\mu_i\,{}^{i}\tilde{x}_i\,r_{ij}d\eta_i$$

$$C_{5ij}'=\int_{L_i}^{L_i+l_i}\mu_i\eta_i{}^{i}\tilde{x}_i\,r_{ij}d\eta_i \qquad C_{6ijk}=\int_{L_i}^{L_i+l_i}\mu_i\,\tilde{r}_{ij}r_{ik}d\eta_i \qquad C_{7i}=\int_{l_i}^{L_i+l_i}\mu_i\eta_i{}^{i}\tilde{x}_i^{T}\,{}^{i}\tilde{x}_id\eta_i$$

$$C_{7i}'=\int_{l_i}^{L_i+l_i}\mu_i\eta_i^{2}{}^{i}\tilde{x}_i^{T}\,{}^{i}\tilde{x}_id\eta_i \qquad C_{8ij}=\int_{L_i}^{L_i+l_i}\mu_i\,{}^{i}\tilde{x}_i^{T}\tilde{r}_{ij}d\eta_i \qquad C_{8ij}'=\int_{L_i}^{L_i+l_i}\mu_i\eta_i{}^{i}\tilde{x}_i^{T}\,\tilde{r}_{ij}d\eta_i\qquad(12-\mathrm{B})$$

$$C_{9ijk}=\int_{L_i}^{L_i+l_i}\mu_i\,\tilde{r}_{ij}^{T}\tilde{r}_{ik}d\eta_i \qquad C_{2i}^{l}=\int_{L_i}^{L_i+l_i}\mu_i\eta_i{}^{i}\tilde{x}_i\,d\eta_i \qquad \alpha_{ij}=C_{5ij}'+\sum_{k=1}^{m(i)}\delta_{ik}C_{6ikj}+\sum_{k=1}^{m'(i)}\delta_{ik}'\tilde{r}_{ik}'\left(\mathrm{L}_i'\right)C_{1ik}$$

$$\beta_{ij}=C_{8ij}'+\sum_{k=1}^{m(i)}\left(\delta_{ik}C_{9ikj}+\delta_{ik}'\tilde{r}_{ik}'^{T}\left(L_i'\right)\tilde{C}_{1ik}\right) \qquad \alpha_{ij}^{l}=B_{0i}^{l}\cdot{}^{i}\tilde{x}_ir_{ij}'\left(L_i'\right)+\sum_{k=1}^{m'(i)}\delta_{ik}'\tilde{r}_{ik}'\left(\mathrm{L}_i'\right)C_{1ik}+\sum_{k=1}^{m(i)}\delta_{ik}\tilde{C}_{1ik}r_{ik}'\left(\mathrm{L}_i'\right)$$

$$\beta_{ij}^{l}=C_{2i}^{l}{}^{T}\tilde{r}_{ij}'\left(L_i'\right)+\sum_{k=1}^{m(i)}\left(\delta_{ik}\tilde{C}_{1ij}^{T}\tilde{r}_{ik}'\left(L_i'\right)+B_{0i}^{1}\cdot\delta_{ik}'\tilde{r}_{ij}'^{T}\left(L_i'\right)\tilde{r}_{ik}'\left(L_i'\right)\right)$$

It should be mentioned that these variables are parts of the Gibbs function (Eq. (12)) which is simplified.

- Potential energy of flexible link

The potential energy caused by the link elasticity is taken as

$$V_H = \frac{1}{2}\sum_{i=1}^{n}\begin{pmatrix}\sum_{j=1}^{m_i'}\sum_{k=1}^{m_i'}\delta_{ij}'(t)\delta_{ik}'(t)K_{ijk}^1\\ +2.\sum_{j=1}^{m_i'}\sum_{k=1}^{m_i}\delta_{ik}'(t)\delta_{ik}(t)K_{ijk}^2\\ +\sum_{j=1}^{m_i'}\sum_{k=1}^{m_i}\delta_{ij}(t)\delta_{ik}(t)K_{ijk}^3\end{pmatrix} \tag{13}$$

where

$$K_{ijk}^1 = \int_{l_i}^{l_i+L_i'}\left[\begin{pmatrix}\mathrm{E}_i\mathrm{I}_{yi}\dfrac{\partial\theta_{yij}'}{\partial\eta}\dfrac{\partial\theta_{yik}'}{\partial\eta}\end{pmatrix}+\begin{pmatrix}\mathrm{E}_i\mathrm{I}_{zi}\dfrac{\partial\theta_{zij}'}{\partial\eta}\dfrac{\partial\theta_{zik}'}{\partial\eta}\end{pmatrix}\right.$$
$$\left.+\begin{pmatrix}\mathrm{E}_i\mathrm{A}_i\dfrac{\partial x_{ij}'}{\partial\eta}\dfrac{\partial x_{ik}'}{\partial\eta}\end{pmatrix}+\begin{pmatrix}\mathrm{G}_i\mathrm{I}_{xi}\dfrac{\partial\theta_{xij}'}{\partial\eta}\dfrac{\partial\theta_{xik}'}{\partial\eta}\end{pmatrix}\right]d\eta \tag{14}$$

$$K_{ijk}^2 = \int_{l_i}^{l_i+L_i'}\left[\begin{pmatrix}\mathrm{E}_i\mathrm{I}_{yi}\dfrac{\partial\theta_{yij}}{\partial\eta}\dfrac{\partial\theta_{yik}'}{\partial\eta}\end{pmatrix}+\begin{pmatrix}\mathrm{E}_i\mathrm{I}_{zi}\dfrac{\partial\theta_{zij}}{\partial\eta}\dfrac{\partial\theta_{zik}'}{\partial\eta}\end{pmatrix}\right.$$
$$\left.+\begin{pmatrix}\mathrm{E}_i\mathrm{A}_i\dfrac{\partial x_{ij}}{\partial\eta}\dfrac{\partial x_{ik}'}{\partial\eta}\end{pmatrix}+\begin{pmatrix}\mathrm{G}_i\mathrm{I}_{xi}\dfrac{\partial\theta_{xij}}{\partial\eta}\dfrac{\partial\theta_{xik}'}{\partial\eta}\end{pmatrix}\right]d\eta \tag{15}$$

$$\mathrm{K}_{ijk}^3 = \int_{l_i}^{l_i+'_i}\left[\begin{pmatrix}\mathrm{E}_i\mathrm{I}_{yi}\dfrac{\partial\theta_{yij}}{\partial\eta}\dfrac{\partial\theta_{yik}}{\partial\eta}\end{pmatrix}+\begin{pmatrix}\mathrm{E}_i\mathrm{I}_{zi}\dfrac{\partial\theta_{zij}}{\partial\eta}\dfrac{\partial\theta_{zik}}{\partial\eta}\end{pmatrix}\right.$$
$$\left.+\begin{pmatrix}\mathrm{E}_i\mathrm{A}_i\dfrac{\partial x_{ij}}{\partial\eta}\dfrac{\partial x_{ik}}{\partial\eta}\end{pmatrix}+\begin{pmatrix}\mathrm{G}_i\mathrm{I}_{xi}\dfrac{\partial\theta_{xij}}{\partial\eta}\dfrac{\partial\theta_{xik}}{\partial\eta}\end{pmatrix}\right]d\eta \tag{16}$$

3.2.3 Derivation of FLM motion equations

By obtaining the Gibbs functions as well as the potential energies of links and hubs, Eqs. (9)–(13), one must differentiate these values with respect to the system generalized quasi-accelerations ($\ddot{\mathbf{q}}$, $\ddot{\boldsymbol{\eta}}$, $\ddot{\boldsymbol{\delta}}$, and $\ddot{\boldsymbol{\delta}}'$):

$$\frac{\partial(S_H+S_L)}{\partial\ddot{q}_j} = \sum_{i=j+1}^{n}\frac{\partial^i\ddot{r}_{O_i}^T}{\partial\ddot{q}_j}\cdot\begin{pmatrix}\left(B_{0i}+B_{0i}'\right)\cdot^i\ddot{r}_{O_i}+\left({}^iB_{1i}+{}^iB_{1i}'\right)+-2\left(B_{2i}+B_{2i}'\right)\cdot^i\omega_i\\ -\left(B_{3i}+B_{3i}'\right)\cdot^i\dot{\omega}_i-{}^i\tilde{\omega}_i\cdot\left(B_{3i}+B_{3i}'\right)\cdot^i\omega_i\end{pmatrix}$$
$$+\sum_{i=j}^{n}\frac{\partial^i\dot{\omega}_i^T}{\partial\ddot{q}_j}\cdot\begin{pmatrix}\left(B_{3i}+B_{3i}'\right)\cdot^i\ddot{r}_{O_i}+\left({}^iB_{6i}+{}^iB_{6i}'\right)+2\left(B_{8i}+B_{8i}'\right)\cdot^i\omega_i\\ +\left(B_{9i}+B_{9i}'\right)\cdot^i\dot{\omega}_i+{}^i\tilde{\omega}_i\cdot\left(B_{9i}+B_{9i}'\right)\cdot^i\omega_i\end{pmatrix} \tag{17}$$

$$\frac{\partial(S_H+S_L)}{\partial\ddot{\delta}_{jf}'} = \sum_{i=j+1}^{n}\frac{\partial^i\ddot{r}_{O_i}^T}{\partial\ddot{\delta}_{jf}'}\cdot\begin{pmatrix}\left(B_{0i}+B_{0i}'\right)\cdot^i\ddot{r}_{O_i}+\left({}^iB_{1i}+{}^iB_{1i}'\right)+-2\left(B_{2i}+B_{2i}'\right)\cdot^i\omega_i\\ -\left(B_{3i}+B_{3i}'\right)\cdot^i\dot{\omega}_i-{}^i\tilde{\omega}_i\cdot\left(B_{3i}+B_{3i}'\right)\cdot^i\omega_i\end{pmatrix}$$
$$+\sum_{i=j+1}^{n}\frac{\partial^i\dot{\omega}_i^T}{\partial\ddot{\delta}_{jf}'}\cdot\begin{pmatrix}\left(B_{3i}+B_{3i}'\right)\cdot^i\ddot{r}_{O_i}+\left({}^iB_{6i}+{}^iB_{6i}'\right)+2\left(B_{8i}+B_{8i}'\right)\cdot^i\omega_i\\ +\left(B_{9i}+B_{9i}'\right)\cdot^i\dot{\omega}_i-{}^i\tilde{\omega}_i\cdot\left(B_{9i}+B_{9i}'\right)\cdot^i\omega_i\end{pmatrix}$$
$$+\sum_{k=1}^{m_j'}\ddot{\delta}_{jk}'\left(C_{3jfk}'+B_{0i}^l\cdot r_{\mathrm{jk}}'^T\left(\mathrm{L}_j'\right)r_{\mathrm{jf}}'\left(\mathrm{L}_j'\right)+\sum_{k=1}^{m_j}\ddot{\delta}_{jk}r_{\mathrm{jk}}'^T\left(\mathrm{L}_j'\right)C_{1jf}\right) \tag{18}$$
$$+2{}^i\omega_j^T\cdot\begin{pmatrix}\dot{\eta}_j{}^j\tilde{x}_j\cdot r_{\mathrm{jk}}'\left(\mathrm{L}_j'\right)-\sum_{k=1}^{m_j}\dot{\delta}_{jk}\tilde{r}_{\mathrm{jk}}'\left(L_j'\right)C_{1jf}\\ -B_{0i}'\cdot\sum_{k=1}^{m_j'}\dot{\delta}_{jk}'\tilde{r}_{\mathrm{jk}}'\left(\mathrm{L}_j'\right)r_{\mathrm{jf}}'\left(\mathrm{L}_j'\right)+\sum_{k=1}^{m_j'}\dot{\delta}_{jk}'C_{4jfk}'\end{pmatrix}+\ddot{\eta}_j\cdot B_{0i}^l\cdot\left({}^jx_j\cdot r_{\mathrm{jk}}'\left(\mathrm{L}_j'\right)\right)$$
$$-{}^j\omega_j^T\cdot\left(\beta_{jf}'+\beta_{jf}^l\right){}^j\omega_j+{}^j\ddot{r}_{O_j}^T\cdot\left(C_{1jf}'+B_{0i}^l\cdot r_{\mathrm{jk}}'\left(\mathrm{L}_j'\right)\right)+{}^j\dot{\omega}_j^T\cdot\left(\alpha_{jf}'+\alpha_{jf}^l\right)$$

$$\begin{aligned}\frac{\partial(S_H+S_L)}{\partial\ddot{\delta}_{jf}} &= \sum_{i=j+1}^{n}\frac{\partial^{i}\ddot{r}_{O_i}^{T}}{\partial\ddot{\delta}_{jf}}\cdot\begin{pmatrix}\left(B_{0i}+B'_{0i}\right)\cdot^{i}\ddot{r}_{O_i}+\left({}^{i}B_{1i}+{}^{i}B'_{1i}\right)+-2\left(B_{2i}+B'_{2i}\right)\cdot^{i}\omega_i\\-\left(B_{3i}+B'_{3i}\right)\cdot^{i}\dot{\omega}_i-{}^{i}\tilde{\omega}_i\cdot\left(B_{3i}+B'_{3i}\right)\cdot^{i}\omega_i\end{pmatrix}\\&+\sum_{i=j+1}^{n}\frac{\partial^{i}\dot{\omega}_i^{T}}{\partial\ddot{\delta}_{jf}}\cdot\begin{pmatrix}\left(B_{3i}+B'_{3i}\right)\cdot^{i}\ddot{r}_{O_i}+\left({}^{i}B_{6i}+{}^{i}B'_{6i}\right)+2\left(B_{8i}+B'_{8i}\right)\cdot^{i}\omega_i\\+\left(B_{9i}+B'_{9i}\right)\cdot^{i}\dot{\omega}_i+{}^{i}\tilde{\omega}_i\cdot\left(B_{9i}+B'_{9i}\right)\cdot^{i}\omega_i\end{pmatrix}\\&+\sum_{k=1}^{m_j}\ddot{\delta}_{jk}\left(C_{4jfk}\right)+\sum_{k=1}^{m'_j}\ddot{\delta}'_{jk}\,r'^{T}_{jk}\left(L'_j\right)C_{1jf}-{}^{i}\omega_j^{T}\cdot\beta_{jf}\,{}^{i}\omega_j+{}^{j}\ddot{r}_{O_j}^{T}\cdot C_{1jf}\\&+2^{j}\omega_j^{T}\cdot\left(\dot{\eta}_j C_{5jf}-\sum_{k=1}^{m_j}\dot{\delta}_{jk}C_{6jfk}-\sum_{k=1}^{m'_j}\dot{\delta}'_{jk}\,\tilde{C}_{1jk}r'_{jf}\left(L'_j\right)\right)+{}^{i}\dot{\omega}_j^{T}\cdot\alpha_{jf}+\ddot{\eta}_j C_{3jf}\end{aligned}\tag{19}$$

$$\begin{aligned}\frac{\partial(S_H+S_L)}{\partial\ddot{\eta}_{\mathrm{j}}} &= \sum_{i=j+1}^{n}\frac{\partial^{i}\ddot{r}_{O_i}^{T}}{\partial\ddot{\eta}_{\mathrm{j}}}\cdot\begin{pmatrix}\left(\mathrm{B}_{0\mathrm{i}}+\mathrm{B}'_{0\mathrm{i}}\right)\cdot^{i}\ddot{r}_{O_i}+\left({}^{i}B_{1\mathrm{i}}+{}^{i}B'_{1\mathrm{i}}\right)+-2\left(\mathrm{B}_{2\mathrm{i}}+\mathrm{B}'_{2\mathrm{i}}\right)\cdot^{i}\omega_{\mathrm{i}}\\-\left(\mathrm{B}_{3\mathrm{i}}+\mathrm{B}'_{3\mathrm{i}}\right)\cdot^{i}\dot{\omega}_{\mathrm{i}}-{}^{i}\tilde{\omega}_{\mathrm{i}}\cdot\left(\mathrm{B}_{3i}+\mathrm{B}'_{3i}\right)\cdot^{i}\omega_{\mathrm{i}}\end{pmatrix}\\&+{}^{j}\ddot{r}_{O_j}^{\mathrm{T}}\cdot\mathrm{B}_{0\mathrm{i}}\,{}^{j}x_{\mathrm{j}}+\mathrm{B}_{0\mathrm{j}}\ddot{\eta}_{\mathrm{j}}+\sum_{\mathrm{k}=1}^{\mathrm{m_j}}\ddot{\delta}_{\mathrm{jk}}\mathrm{C}_{3\mathrm{jk}}+\sum_{\mathrm{k}=1}^{\mathrm{m'_j}}\ddot{\delta}'_{\mathrm{jk}}\,\mathrm{B}'^{\,j}_{0i}\,{}^{j}x_{\mathrm{j}}^{\mathrm{T}}\cdot r'_{jk}\left(\mathrm{L}'_{\mathrm{j}}\right)\\&-2^{i}\omega_{\mathrm{j}}^{\mathrm{T}}\cdot\left(\sum_{\mathrm{k}=1}^{\mathrm{m_j}}\dot{\delta}_{\mathrm{jk}}\,\mathrm{C}_{5\mathrm{jk}}+\sum_{\mathrm{k}=1}^{\mathrm{m'_j}}\dot{\delta}'_{\mathrm{jk}}\,\mathrm{B}'^{\,j}_{0i}\,{}^{j}\tilde{x}_{j}\cdot r'_{jk}\left(\mathrm{L}'_{\mathrm{j}}\right)\right)-{}^{i}\dot{\omega}_{\mathrm{j}}^{\mathrm{T}}\cdot\left(\sum_{\mathrm{k}=1}^{\mathrm{m_j}}\delta_{\mathrm{jk}}\mathrm{C}_{5\mathrm{jk}}+\sum_{\mathrm{k}=1}^{\mathrm{m'_j}}\delta'_{\mathrm{jk}}\mathrm{B}'^{\,j}_{0i}\,{}^{j}\tilde{x}_{j}.r'_{jk}\left(\mathrm{L}'_{\mathrm{j}}\right)\right)\\&-{}^{j}\omega_{\mathrm{j}}^{\mathrm{T}}\cdot\left(\sum_{\mathrm{k}=1}^{\mathrm{m_j}}\delta_{\mathrm{jk}}\mathrm{C}_{8\mathrm{jk}}^{\mathrm{T}}+\mathrm{C}_{7\mathrm{j}}+\sum_{\mathrm{k}=1}^{\mathrm{m'_j}}\delta'_{\mathrm{jk}}\mathrm{B}'^{\,j}_{0i}\,{}^{\prime\mathrm{T}}\tilde{r}'_{jk}\left(\mathrm{L}'_{\mathrm{j}}\right)^{j}\tilde{x}_{j}\right)^{j}\omega_{\mathrm{j}}\end{aligned}\tag{20}$$

$$\frac{\partial(V_H+V_L)}{\partial\dot{\delta}'_{jf}}=\sum_{\mathrm{k}=1}^{\mathrm{m_j}}\dot{\delta}'_{\mathrm{jk}}(\mathrm{t})K'_{\mathrm{jkf}}+\sum_{\mathrm{k}=1}^{\mathrm{m'_j}}\dot{\delta}'_{\mathrm{jk}}(\mathrm{t})K^{1}_{\mathrm{jkf}}+2.\sum_{\mathrm{k}=1}^{\mathrm{m_j}}\delta_{\mathrm{jk}}(\mathrm{t})K^{2}_{jkf}\tag{21}$$

$$\frac{\partial(V_H+V_L)}{\partial\delta_{jf}}=\sum_{\mathrm{k}=1}^{\mathrm{m_j}}\delta_{\mathrm{jk}}(\mathrm{t})K^{3}_{\mathrm{jkf}}+2.\sum_{\mathrm{k}=1}^{\mathrm{m'_j}}\delta'_{\mathrm{jk}}(\mathrm{t})K^{2}_{jkf}\tag{22}$$

where the values of ${}^{i}\ddot{\mathbf{r}}_{O_i}$ and ${}^{i}\dot{\boldsymbol{\omega}}_i$ are recursively found in Eqs. (6) and (7). To perform differentiation, one should first rewrite these terms in summation form.

$${}^{i}\ddot{\mathbf{r}}_{O_i}=\sum_{k=1}^{i-1}{}^{i}\mathbf{R}_k\left({}^{k}\ddot{\mathbf{r}}_{O_{k+1}/\mathrm{O_k}}+{}^{k}\dot{\boldsymbol{\omega}}_k\times{}^{k}\mathbf{r}_{O_{k+1}/O_k}+{}^{k}\boldsymbol{\omega}_k\times\left(2^{k}\dot{\mathbf{r}}_{O_{k+1}/O_k}+{}^{k}\boldsymbol{\omega}_k\times{}^{k}\mathbf{r}_{O_{k+1}/O_k}\right)\right)+{}^{i}\mathbf{R}_0 g^{0}\mathbf{y}_0\tag{23}$$

$${}^{i}\dot{\omega}_i=\sum_{\mathrm{k}=1}^{i-1}{}^{i}R_k\left({}^{k}\ddot{\theta}_k+{}^{k}\omega_k\times{}^{k}\dot{\theta}_k\right)+{}^{i}R_k\left({}^{i}\omega_k+{}^{k}\dot{\theta}_k\right)\times{}^{i}R_{k+1}{}^{\mathrm{k+1}}z_{k+1}\dot{q}_{k+1}+\sum_{\mathrm{k}=1}^{\mathrm{i}}{}^{i}R_k{}^{k}z_k\ddot{q}_k\tag{24}$$

To differentiate Eqs. (23) and (24), the obtained terms can be classified based on whether they are functions of generalized pseudo-accelerations (Appendix A). Furthermore, the values of the vectors ${}^{i}\ddot{\mathbf{r}}_{O_i}$ and ${}^{i}\dot{\boldsymbol{\omega}}_i$ including the generalized pseudo-accelerations can be written in the summation form using Eqs. (23) and (24) as in

$${}^{\mathrm{i}}\ddot{\mathbf{r}}_{O_{s,i}}=\sum_{k=1}^{i-1}{}^{i}\mathbf{R}_k\left({}^{k}\ddot{\mathbf{r}}_{O_{k+1}/O_k}+{}^{k}\dot{\boldsymbol{\omega}}_{s,k}\times{}^{k}\mathbf{r}_{O_{k+1}/O_k}\right)\tag{25}$$

$${}^{i}\dot{\boldsymbol{\omega}}_{\mathrm{s,i}}=\sum_{\mathrm{k}=1}^{\mathrm{i}}{}^{i}\mathbf{R}_{\mathrm{k}}{}^{k}\mathbf{z}_{\mathrm{k}}\ddot{\mathrm{q}}_{\mathrm{k}}+\sum_{\mathrm{k}=1}^{\mathrm{i-1}}{}^{i}\mathbf{R}_{\mathrm{k}}\,{}^{k}\ddot{\boldsymbol{\theta}}_{\mathrm{k}}(\mathrm{L_k}+\mathrm{l_k})\tag{26}$$

The remaining terms of Eqs. (23) and (24) that are not mentioned in Eqs. (25) and (26) are defined as ${}^{i}\ddot{\mathbf{r}}_{\mathrm{O_{v,i}}}$ and ${}^{i}\dot{\boldsymbol{\omega}}_{\mathrm{v,i}}$. The general form of system motion equations based on the G-A formulation is found after substitution of the values of equations in Appendix A into Eqs. (17)–(22) in the form

$$\begin{aligned}&\frac{\partial(S_H+S_L)}{\partial\Theta}+\frac{\partial(V_H+V_L)}{\partial\Theta}=\Gamma.\\&\text{where}:\Theta=[q_1,\dot{\delta}'_{11},\ldots,\dot{\delta}'_{1m_1},\delta_{11},\ldots,\delta_{1m_1},\ldots,q_n,\\&\qquad\dot{\delta}'_{n1},\ldots,\dot{\delta}'_{nm_n},\delta_{n1},\ldots,\delta_{nm_n},\eta_{1,}\ldots\eta_n]^{T}\\&\qquad\Gamma=[\tau_1,0,..,\tau_n,0,..,F_1,..,F_n]\end{aligned}\tag{27}$$

By categorizing Eq. (27) and transferring the terms in the left-hand side of this equation that are not functions of generalized quasi-accelerations to the right-hand side, and after some reformatting, the final form of system coupled forward dynamic equations can be obtained.

$$\mathbf{I}\left(\boldsymbol{\Theta},\dot{\boldsymbol{\Theta}}\right)\ddot{\boldsymbol{\Theta}}=\mathbf{Re}+\boldsymbol{\Gamma}\tag{28}$$

- Inertia matrix ($\mathbf{I}(\boldsymbol{\Theta}, \dot{\boldsymbol{\Theta}})$)

The elements of system inertia matrix is found by putting together the terms in Eq. (27) based on the vector $\boldsymbol{\Theta}$.

- Quasi-acceleration coefficients of the coupled equation of revolute joint

$$
\begin{aligned}
&\left(\sum_{k=1}^{n} {}^{j}z_j^T \times \left({}^{j}\sigma_k - {}^{j}\psi_k + {}^{j}\sigma_k' - {}^{j}\psi_k'\right)^{k} z_k - \sum_{k=1}^{n-1} {}^{j}z_j^T \times \left({}^{j}U_k'\right)^{k} z_k\right)\ddot{q}_k \\
&\quad + \begin{pmatrix} \sum_{k=1}^{n-1}\sum_{t=1}^{m(i)} {}^{j}z_j^T \times \left({}^{j}\sigma_{k+} - {}^{j}\psi_{k+}\right)\theta_{kt} + \sum_{k=1}^{n-1}\sum_{t=1}^{m(i)} {}^{j}z_j^T \times \left({}^{j}\xi_{k+} + {}^{j}\gamma_k\right) r_{kt} \\ -\sum_{k=1}^{n-2}\sum_{t=1}^{m(i)} {}^{j}z_j^T \times {}^{j}U_{k+}\theta_{kt} + \sum_{k=j+1}^{n}\sum_{t=1}^{m(i)} {}^{j}z_j^T \times {}^{j}\tilde{r}_{0_k/0_j}\, {}^{j}R_k C_{1kt} + \sum_{k=j}^{n}\sum_{t=1}^{m(i)} {}^{j}z_j^T \times {}^{j}R_k \alpha_{kt} \end{pmatrix} \ddot{\delta}_{kt} \\
&\quad + \begin{pmatrix} \sum_{k=1}^{n-1}\sum_{t=1}^{m'(i)} {}^{j}z_j^T \times \left({}^{j}\sigma_{k+}' - {}^{j}\psi_{k+}' + {}^{j}\sigma_{k+} - {}^{j}\psi_{k+}\right)\theta_{kt}' + \sum_{k=1}^{n-1}\sum_{t=1}^{m'(i)} {}^{j}z_j^T \times \left({}^{j}\xi_{k+}' + {}^{j}\gamma_k' + {}^{j}\xi_{k+} + {}^{j}\gamma_k\right) r_{kt}' \\ -\sum_{k=1}^{n-2}\sum_{t=1}^{m'(i)} {}^{j}z_j^T \times \left({}^{j}U_{k+}' + {}^{j}U_{k+}\right)\theta_{kt}' + \sum_{k=j+1}^{n}\sum_{t=1}^{m'(i)} {}^{j}z_j^T \times {}^{j}\tilde{r}_{O_k/O_j}\, {}^{j}R_k \left(C_{1kt}' + B_{0_j}^{l}\, r_{kt}'\left(L_j'\right)\right) \\ +\sum_{k=j}^{n}\sum_{t=1}^{m'(i)} {}^{j}z_j^T \times {}^{j}R_k \left(\alpha_{kt}' + \alpha_{kt}^{l}\right) \end{pmatrix} \ddot{\delta}_{kt}' \\
&\quad + \begin{pmatrix} \sum_{k=1}^{n-1}{}^{j}z_j^T \times \left({}^{j}\xi_{k+} {}^{j}\gamma_k\right)^{k} x_k - \sum_{k-j}^{n} {}^{j}z_j^T \times {}^{j}R_k \left(\sum_{t=1}^{m(i)} \delta_{kt} C_{5kt} + \sum_{t=1}^{m'(i)} \delta_{kt}' B_{0j}^{l}\, {}^{j}\tilde{r}_j r_{kt}'\left(L_j'\right)\right) \\ +\sum_{k=j+1}^{n} {}^{j}z_j^T \times {}^{j}\tilde{r}_{O_k/O_j}\, {}^{j}R_k B_{0k}\, {}^{k}x_k \end{pmatrix} \ddot{\eta}_k
\end{aligned}
\tag{29}
$$

where

$$
{}^{j}\sigma_k = \sum_{i=\max(k,j)}^{n} {}^{j}R_i B_{9i}\, {}^{i}R_k \qquad {}^{j}\psi_k = \sum_{i=max(k,j+1)}^{n} {}^{j}\tilde{r}_{O_i/O_j}\, {}^{j}R_i B_{3i}\, {}^{i}R_k \qquad {}^{j}U_k = \sum_{t=k}^{n=1} \left({}^{j}\gamma_t + {}^{j}\xi_{t+}\right) {}^{t}\tilde{r}_{O_{t+1}/O_t}\, {}^{t}R_k
$$

$$
{}^{j}\sigma_{k^+} = \sum_{i=\max(k+1,j)}^{n} {}^{j}R_i B_{9i}\, {}^{i}R_k \qquad {}^{j}\psi_{k^+} = \sum_{i=max(k+1,j+1)}^{n} {}^{j}\tilde{r}_{O_i/O_j}\, {}^{j}R_i B_{3i}\, {}^{i}R_k \qquad {}^{j}U_{k^+} = \sum_{t=k+1}^{n-1} \left({}^{j}\gamma_t + {}^{j}\xi_{t^+}\right) {}^{t}\tilde{r}_{O_{t+1}/O_t}\, {}^{t}R_k
$$

$$
{}^{j}\sigma_k' = \sum_{i=\max(k,j)}^{n} {}^{j}R_i B_{9i}'\, {}^{i}\mathrm{R}_k \qquad {}^{j}\psi_k' = \sum_{i=\max(k,j+1)}^{n} {}^{j}\tilde{r}_{O_i/O_j}\, {}^{j}R_i B_{3i}'\, {}^{i}R_k \qquad {}^{j}U_k' = \sum_{t=k}^{n-1} \left({}^{j}\gamma_t' + {}^{j}\xi_{t^+}'\right) {}^{t}\tilde{r}_{O_{t+1}/O_t}\, {}^{t}R_k
$$

$$
{}^{j}\gamma_t = \sum_{i=\max(t+1,j+1)}^{n} {}^{j}\tilde{r}_{O_i/O_j} B_{0i}\, {}^{j}R_t \qquad {}^{j}\xi_{t^+} = \sum_{i=\max(t+1,j)}^{n} {}^{j}R_i B_{3i}\, {}^{i}R_t \qquad {}^{j}\gamma_t' = \sum_{i=\max(t+1,j+1)}^{n} {}^{j}\tilde{r}_{O_i/O_j} B_{0i}'\, {}^{j}R_t
$$

$$
{}^{j}\xi_{t^+}' = \sum_{i=\max(t+1,j)}^{n} {}^{j}R_i B_{3i}'\, {}^{i}R_t
$$

where, ${}^{j}\tilde{\mathbf{r}}_{O_i/O_j}$ is the skew-symmetric matrix related to the vector ${}^{j}\mathbf{r}_{O_i/O_j}$.

- Quasi-acceleration coefficients of the couple equation of link deformation

Owing to the symmetricity of system inertia matrix, the coefficient of $\ddot{q}_k$ in the equation of deformation is equivalent to the coefficient of $\ddot{\delta}_{kt}$ in Eq. (29).

$$
\begin{aligned}
&\begin{pmatrix} \sum_{k=1}^{n-1}\sum_{t=1}^{m(i)} \theta_{jf}^T \times \left({}^{j+}\sigma_{k^+} - {}^{j+}\psi_{k^+}\right)\theta_{kt} - \sum_{k=1}^{n-2}\sum_{t=1}^{m(i)} \theta_{jf}^T \times {}^{j+}U_{k^+}\theta_{kt} \\ -\sum_{k=1}^{n-2}\sum_{t=1}^{m(i)} r_{jf}^T \times {}^{j}V_k\theta_{kt} - \sum_{k=1}^{n-1}\sum_{t=1}^{m(i)} r_{jf}^T \times {}^{j+}\xi_{k^+}\theta_{kt} - \sum_{k=1}^{j-2}\sum_{t=1}^{m(i)} C_{ljf}^T \times {}^{j}W_k\theta_{kt} \\ +\sum_{k=1}^{j-l}\sum_{t=1}^{m(i)} \alpha_{jf}^T \times {}^{j}R_k\theta_{kt} + \sum_{t=1}^{m(i)} C_{4kfi} + \sum_{k=1}^{n-1}\sum_{t=1}^{m(i)} \theta_{jf}^T \times \left({}^{j+}\gamma_k + {}^{j+}\xi_{k^+}\right) r_{kt} + \sum_{k=1}^{n-1}\sum_{t=1}^{m(i)} r_{jf}^T \times {}^{j}\lambda_k r_{kt} + \sum_{k=j+1}^{n}\sum_{t=1}^{m(i)} \theta_{jf}^T \times {}^{j}R_k\alpha_{kt} \\ +\sum_{k=1}^{j-1}\sum_{t=1}^{m(i)} C_{1jf}^T \times {}^{j}R_k r_{kt} + \sum_{k=j+1}^{n}\sum_{t=1}^{m(i)} r_{jf}^T \times {}^{j}R_k C_{1kt} + \sum_{k=j+2}^{n}\sum_{t=1}^{m(i)} \theta_{jf}^T \times {}^{j}\tilde{r}_{O_k/O_{j+1}}\, {}^{j}R_k C_{1kt} \end{pmatrix} \ddot{\delta}_{kt} \\
&+ \begin{pmatrix} \sum_{k=1}^{n-1}\sum_{t=1}^{m'(i)} \theta_{jf}^T \times \left({}^{j+}\sigma_{k^+} - {}^{j+}\psi_{k^+}\right)\theta_{kt}'\left(L_k'\right) - \sum_{k=1}^{n-2}\sum_{t=1}^{m'(i)} \theta_{jf}^T \times {}^{j+}U_{k^+}\,\theta_{kt}'\left(L_k'\right) - \sum_{k=1}^{n-2}\sum_{t=1}^{m'(i)} r_{jf}^T \times {}^{j}V_k\theta_{kt}'\left(L_k'\right) \\ -\sum_{k=1}^{n-1}\sum_{t=1}^{m'(i)} r_{jf}^T \times {}^{j+}\xi_{k^+}\theta_{kt}'(L'k) - \sum_{k=1}^{j-2}\sum_{t=1}^{m'(i)} C_{1jf}^T \times {}^{j}W_k\theta_{kt}'\left(L_k'\right) + \sum_{k=1}^{j-1}\sum_{t=1}^{m'(i)} \alpha_{jf}^T \times {}^{j}R_k\theta_{kt}'\left(L_k'\right) \\ +\sum_{t=1}^{m'(i)} r_{jf}'^T\left(L_k'\right) \times C_{1kt} + \sum_{k=1}^{n-1}\sum_{t=1}^{m'(i)} \theta_{jf}^T \times \left({}^{j+}\gamma_k + {}^{j+}\xi_{k^+}\right) r_{kt}'\left(L_k'\right) + \sum_{k=1}^{n-1}\sum_{t=1}^{m'(i)} r_{jf}^T \times {}^{j}\lambda_k r_{kt}'\left(L_k'\right) \\ +\sum_{k=1}^{j-l}\sum_{t=1}^{m'(i)} C_{1jf}^T \times {}^{j}R_k r_{kt}'\left(L_k'\right) + \sum_{k=j+1}^{n}\sum_{t=1}^{m'(i)} r_{jf}^T \times {}^{j}R_k B_{0k}^{l} r_{kt}'\left(L_k'\right) + \sum_{k=j+1}^{n}\sum_{t=1}^{m'(i)} \theta_{jf}^T \times {}^{j}R_k\alpha_{kt}^{l} \\ +\sum_{k=j+2}^{n}\sum_{t=1}^{m'(i)} \theta_{jf}'^T \times {}^{j}\tilde{r}_{O_k/O_{j+1}}\, {}^{j}R_k B_{0j}^{l} r_{kt}'\left(L_k'\right) \end{pmatrix} \ddot{\delta}_{kt}' \\
&+ \begin{pmatrix} +\sum_{k=1}^{n-1} \theta_{jf}^T \times \left({}^{j+}\gamma_k + {}^{j+}\xi_{k^+}\right)^{k} x_k + \sum_{k=j+1}^{n} r_{jf}^T \times {}^{j}R_k B_{0k}\, {}^{k}\mathrm{x}_k + \sum_{k=j+2}^{n} \theta_{jf}^T \times {}^{j}\tilde{r}_{O_k/O_{j+1}}\, {}^{j}R_k B_{0k}\, {}^{k}x_k \\ +\sum_{k=1}^{n-1} r_{jf}^T \times {}^{j}\lambda_k\, {}^{k}x_k + \sum_{k=1}^{j-l} C_{1jf}^T \times {}^{j}R_k\, {}^{k}x_k + C_{3kf} - \sum_{k=j+1}^{n} \theta_{jf}^T \times {}^{j}R_k \begin{pmatrix} \sum_{t=1}^{m(i)} \delta_{kt} C_{5kt} \\ +\sum_{t=1}^{m'(i)} \delta_{kt}' B_{0j}^{l}\, {}^{k}\tilde{x}_k r_{kt}'\left(L_k'\right) \end{pmatrix} \end{pmatrix} \ddot{\eta}_k
\end{aligned}
\tag{30}
$$

where

$$
\begin{aligned}
{}^{j+}\sigma_{k^+} &= \sum_{i=\max(k+1,j+1)}^{n} {}^{j}R_i B_{9i}\, {}^{i}R_k {}^{j+}\xi_{k^+} = \sum_{i=\max(k+1,j+1)}^{n} {}^{j}R_i B_{3i}\, {}^{i}R_k {}^{j}V_k = \sum_{t=k+1}^{n-1} {}^{j}\lambda_t {}^{t}\tilde{r}_{O_{t+1}/O_t} {}^{t}R_k {}^{j}V'_k = \sum_{t=k+1}^{n-1} {}^{j}\lambda'_t {}^{t}\tilde{r}_{O_{t+1}/O_t} {}^{t}R_k {}^{j+}\psi_{k^+} \\
&= \sum_{i=\max(k+1,j+2)}^{n} {}^{j}\tilde{r}_{O_i/O_{j+1}} {}^{j}R_i B_{3i}\, {}^{i}R_k {}^{j+}\gamma_k = \sum_{i=\max(k+1,j+2)}^{n} {}^{j}\tilde{r}_{O_i/O_{j+1}} B_{0i}\, {}^{t}R_k {}^{j}W_k = \sum_{t=k+1}^{j-1} {}^{j}R_t {}^{t}\tilde{r}_{O_{t+1}/O_t} {}^{t}R_k {}^{j+}U_{k^+} \\
&= \sum_{t=k+1}^{n-1} \left({}^{j+}\gamma_t + {}^{j+}\xi_{t^+}\right) {}^{t}\tilde{r}_{O_{t+1}/O_t} {}^{t}R_k {}^{j+}\lambda_k = \sum_{i=\max(k+1,j+1)}^{n} B_{0i}\, {}^{t}R_k
\end{aligned}
$$

- Quasi-acceleration coefficients of the coupled equation of hub deformation

$$
\begin{pmatrix}
\sum_{k=1}^{n-1}\sum_{t=1}^{m'(i)} \theta'^{T}_{jf} \times \left({}^{j+}\sigma_{k^+} - {}^{j+}\psi_{k^+} + {}^{j+}\sigma'_{k^+} - {}^{j+}\psi'_{k^+}\right)\theta'_{kt} - \sum_{k=1}^{n-2}\sum_{t=1}^{m'(i)} \theta'^{T}_{jf} \times \left({}^{j+}U_{k^+} + {}^{j+}U'_{k^+}\right)\theta'_{kt} \\
-\sum_{k=1}^{n-2}\sum_{t=1}^{m'(i)} r'^{T}_{jf} \times \left({}^{j}V'_k + {}^{j}V_k\right)\theta'_{kt} + \sum_{k=1}^{n-1}\sum_{t=1}^{m'(i)} r'^{T}_{jf} \times \left({}^{j}\lambda'_k + {}^{j}\lambda_k\right) r'_{kt} \\
-\sum_{k=1}^{n-1}\sum_{t=1}^{m'(i)} r'^{T}_{jf} \times \left({}^{j+}\xi_{k^+} + {}^{j+}\xi'_{k^+}\right)\theta'_{kt} - \sum_{k=1}^{j-2}\sum_{t=1}^{m'(i)} C'^{T}_{1jf} \times \left({}^{j}W_k + {}^{j}W'_k\right)\theta'_{kt} \\
+\sum_{k=1}^{j-1}\sum_{t=1}^{m'(i)} \left(\alpha'^{T}_{jf} + \alpha^{l\,T}_{jf}\right) \times {}^{j}R_k \theta'_{kt} + \sum_{k=j+1}^{n}\sum_{t=1}^{m'(i)} \theta'^{T}_{jf} \times {}^{j}R_k \left(\alpha'_{kt} + \alpha^{l}_{kt}\right) \\
+\sum_{t=1}^{m'(i)} \left(C'_{3kft} + \left(\mathrm{B}^{l}_{0k} r'^{T}_{jf} r'_{kt}\right)\right) + \sum_{k=1}^{n-1}\sum_{t=1}^{m'(i)} \theta'^{T}_{jf} \times \left({}^{j+}\gamma'_k + {}^{j+}\xi'_{k^+} + {}^{j+}\gamma'_k + {}^{j+}\xi'_{k^+}\right) r'_{kt} \\
+\sum_{k=1}^{j-1}\sum_{t=1}^{m'(i)} \left(C'^{T}_{1jf} + \mathrm{B}^{l}_{0k} r'^{T}_{jf}\right) \times {}^{j}R_k r'_{kt} + \sum_{k=j+1}^{n}\sum_{t=1}^{m'(i)} r'^{T}_{jf} \times {}^{j}R_k \left(C'_{1kt} + \mathrm{B}^{l}_{0k} r'_{kt}\right) \\
+\sum_{k=j+2}^{n}\sum_{t=1}^{m'(i)} \theta'^{T}_{jf} \times {}^{j}\tilde{r}_{O_k/O_{j+1}} {}^{j}R_k \left(C'_{1kt} + \mathrm{B}^{l}_{0k} r'_{kt}\right)
\end{pmatrix} \ddot{\delta}'_{kt}
$$

$$
+ \begin{pmatrix}
\sum_{k=1}^{n-1} \theta'^{T}_{jf} \times \left({}^{j+}\gamma_k + {}^{j+}\xi_{k^+}\right)^{k} x_k + \sum_{k=j+1}^{n} r'^{T}_{jf} \times {}^{j}R_k B_{0k}\, {}^{k}x_k + \sum_{k=j+2}^{n} \theta'^{T}_{jf} \times {}^{j}\tilde{r}_{O_k/O_{j+1}} {}^{j}R_k B_{0k}\, {}^{k}x_k \\
+\sum_{k=1}^{n-1} r'^{T}_{jf} \times {}^{j}\lambda_k {}^{k}x_k + \sum_{k=1}^{j-1} B^{l}_{0k} r'^{T}_{jf} \times {}^{j}R_k {}^{k}x_k + B^{l}_{0k}\, {}^{k}x^{T}_{k} r'_{kt} - \sum_{k=j+1}^{n} \theta'^{T}_{jf} \times {}^{j}R_k \begin{pmatrix} \sum_{t=1}^{m(i)} \delta_{kt} C_{5kt} \\ +\sum_{t=1}^{m'(i)} \delta'_{kt} B^{l}_{0j}\, {}^{k}\tilde{x}_k r'_{kt} \left(L'_k\right) \end{pmatrix}
\end{pmatrix} \ddot{\eta}_k \tag{31}
$$

- Quasi-acceleration coefficients of the coupled equation of prismatic joint

$$
\left(\sum_{k=1}^{n-1} {}^{j}x^{T}_{j} \times {}^{j}\lambda_k {}^{k}x_k + \sum_{k=j+1}^{n} {}^{j}x^{T}_{j} \times {}^{j}R_k B_{0k}\, {}^{k}x_k + \sum_{k=1}^{j-1} {}^{j}x^{T}_{j} \times {}^{j}R_k B_{0j}\, {}^{k}x_k + B_{0k}\right) \ddot{\eta}_k \tag{32}
$$

- Vector of remaining force and terms (**Re**)

The external forces exerted to the system, forces and torques applied from the motors (inputs), and the terms from the left-hand side of dynamic equations (Eq. (27)) that are not functions of pseudo-accelerations and have been transferred to the right-hand side constitute the vector of remaining force and terms in the form

$$
\begin{aligned}
Re_{qj} &= \tau_j - \sum_{i=j+1}^{n} \frac{\partial {}^{i}\ddot{r}^{T}_{O_i}}{\partial \ddot{q}_j} \times {}^{i}S_i - \sum_{i=j}^{n} \frac{\partial {}^{i}\dot{\omega}^{T}_{i}}{\partial \ddot{q}_j} \\
&\quad \times {}^{i}T_i - \sum_{i=j+1}^{n} \frac{\partial {}^{i}\ddot{r}^{T}_{O_i}}{\partial \ddot{q}_j} \times {}^{i}S'_i - \sum_{i=j}^{n} \frac{\partial {}^{i}\dot{\omega}^{T}_{i}}{\partial \ddot{q}_j} \times {}^{i}T'_i
\end{aligned} \tag{33}
$$

$$
Re_{\delta_{jf}} = Q_{jf} - \sum_{i=j+1}^{n} \frac{\partial {}^{i}\ddot{r}^{T}_{O_i}}{\partial \ddot{\delta}_{jf}} \times {}^{i}S_i - \sum_{i=j+1}^{n} \frac{\partial {}^{i}\dot{\omega}^{T}_{i}}{\partial \ddot{\delta}_{jf}} \times {}^{i}T_i \tag{34}
$$

$$
\begin{aligned}
Re_{\delta'_{jf}} &= Q^{s}_{jf} + Q^{l}_{jf} - \sum_{i=j+1}^{n} \frac{\partial {}^{i}\ddot{r}^{T}_{O_i}}{\partial \ddot{\delta}_{jf}} \times {}^{i}S_i - \sum_{i=j+1}^{n} \frac{\partial {}^{i}\dot{\omega}^{T}_{i}}{\partial \ddot{\delta}_{jf}} \\
&\quad \times {}^{i}T_i - \sum_{i=j+1}^{n} \frac{\partial {}^{i}\ddot{r}^{T}_{O_i}}{\partial \ddot{\delta}_{jf}} \times {}^{i}S'_i \sum_{i=j+1}^{n} \frac{\partial {}^{i}\dot{\omega}^{T}_{i}}{\partial \ddot{\delta}_{jf}} \times {}^{i}T'_i
\end{aligned} \tag{35}
$$

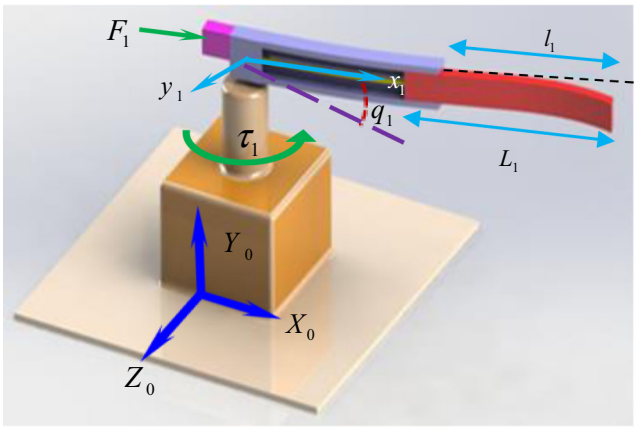

Fig. 5 Single-link flexible manipulator with R-P joint

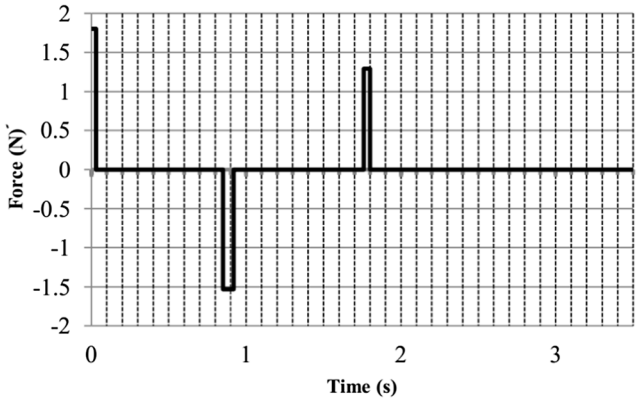

Fig. 6 Prismatic joint imported force

$$Re_{\eta_j} = F_j + Q_j^{'} - \sum_{i=j+1}^{n} \frac{\partial^i r^{\cdot\cdot T}_{O_i}}{\partial \eta^{\cdot\cdot}_j} \times {}^i S_i \tag{36}$$

in which

$${}^i\mathbf{S}_i = \mathrm{B}_{0i}\,{}^i\ddot{\mathbf{r}}_{\mathrm{O_{v,i}}} - \mathbf{2}\boldsymbol{B}_{2i}\,{}^i\boldsymbol{\omega}_i - \mathrm{B}_{3i}\,{}^i\dot{\boldsymbol{\omega}}_{\mathrm{v,i}} - {}^i\tilde{\boldsymbol{\omega}}_i \mathrm{B}_{3i}\,{}^i\boldsymbol{\omega}_i \tag{37}$$

$${}^i\mathbf{T}_i = \mathrm{B}_{3i}\,{}^i\ddot{\mathbf{r}}_{\mathrm{O_{v,i}}} + \mathbf{2}\boldsymbol{B}_{8i}\,{}^i\boldsymbol{\omega}_i + \mathrm{B}_{9i}\,{}^i\dot{\boldsymbol{\omega}}_{\mathrm{v,i}} + {}^i\tilde{\boldsymbol{\omega}}_i \mathrm{B}_{9i}\,{}^i\boldsymbol{\omega}_i \tag{38}$$

$${}^iS_i^{'} = B_{0i}^{'}\,{}^i\ddot{r}_{0_{v,i}} - 2B_{2i}^{'}\,{}^i\omega_i - B_{3i}^{'}\,{}^i\dot{\omega}_{v,i} - {}^i\tilde{\omega}_i B_{3i}^{'}\,{}^i\omega_i \tag{39}$$

$${}^iT_i^{'} = B_{3i}^{'}\,{}^i\ddot{r}_{0_{v,i}} + 2B_{8i}^{'}\,{}^i\omega_i + B_{9i}^{'}\,{}^i\dot{\omega}_{v,i} + {}^i\tilde{\omega}_i B_{9i}^{'}\,{}^i\omega_i \tag{40}$$

$$\begin{aligned} Q_{jf} = & -\left(\sum_{k=1}^{m_j}\delta_{jk}(t)K_{jkf}^3 + 2.\sum_{k=1}^{m_j^{'}}\delta_{jk}^{'}(t)K_{jkf}^2\right) + \left({}^j\omega_j^T \times \beta_{jf}\,{}^j\omega_j\right) - \left({}^j\ddot{r}_{O_{v,j}}^T \times C_{1jf}\right) \\ & - \left({}^j\dot{\omega}_{v,j}^T \times \alpha_{jf}\right) - 2\,{}^j\omega_j^T \times \left(\dot{\eta}_j C_{5jf} - \sum_{k=1}^{m_j}\dot{\delta}_{jk} C_{6jfk} - \sum_{k=1}^{m_j^{'}}\dot{\delta}_{jk}^{'} \tilde{C}_{1jk} r_{jk}^{'}\right) \end{aligned} \tag{41}$$

$$\begin{aligned} Q_{jf}^s = & -\left(\sum_{k=1}^{m_j}\delta_{jk}^{'}(t)K_{jkf}^{'}\right) - 2\,{}^j\omega_j^T \times \left(-\sum_{k=1}^{m_j^{'}}\dot{\delta}_{jk}^{'} C_{4jfk}\right) + \left({}^j\omega_j^T \times \beta_{jf}^{'}\,{}^j\omega_j\right) - \left({}^j\ddot{r}_{O_{v,j}}^T \times C_{1jf}^{'}\right) \\ & - \left({}^j\dot{\omega}_{v,j}^T \times \alpha_{jf}^{'}\right) \end{aligned} \tag{42}$$

$$\begin{aligned} Q_{jf}^l = & -\left(\sum_{k=1}^{m_j^{'}}\delta_{jk}^{'}(t)K_{jkf}^1 + 2.\sum_{k=1}^{m_j}\delta_{jk}(t)K_{jkf}^2\right) + \left({}^j\omega_j^T \times \beta_{jf}^l\,{}^j\omega_j\right) - \left\{{}^j\ddot{r}_{O_{v,j}}^T \times \left(B_{j0}^l r_{jf}^{'}(L_j)\right)\right\} \\ & - 2\,{}^j\omega_j^T \times \left(\dot{\eta}_j\,{}^j\tilde{x}_j r_{jf}^{'}(L_j) - \sum_{k=1}^{m_j}\dot{\delta}_{jk}\tilde{r}_{jk}^{'}(L_j) C_{1jf} - B_{j0}^l \sum_{k=1}^{m_j^{'}}\dot{\delta}_{jk}^{'}\tilde{r}_{jf}^{'}(L_j) r_{jf}^{'}(L_j)\right) - \left({}^j\dot{\omega}_{v,j}^T \times \alpha_{jf}^{l}\right) \end{aligned} \tag{43}$$

$$\begin{aligned} Q_j^{'} = & -{}^j x_j^T \times B_{0j}\,{}^j\ddot{r}_{O_{v,j}} + 2\,{}^j\omega_j^T \times \\ & \left(\sum_{k=1}^{m_j}\dot{\delta}_{jk} C_{5jk} + B_{j0}^l \sum_{k=1}^{m_j^{'}}\dot{\delta}_{jk}^{'}\,{}^j\tilde{x}_j r_{jf}^{'}(L_j)\right) \\ & + {}^j\dot{\omega}_{v,j}^T \times \left(\sum_{k=1}^{m_j}\delta_{jk} C_{5jk} + B_{j0}^l \sum_{k=1}^{m_j^{'}}\delta_{jk}^{'}\,{}^j\tilde{x}_j r_{jf}^{'}(L_j)\right) \\ & + {}^j\omega_j^T \times \left(\sum_{k=1}^{m_j}\delta_{jk} C_{8jk}^T + C_{7j} + B_{j0}^l \sum_{k=1}^{m_j}\delta_{jk} r_{jf}^{'T}(L_j)\,{}^j\tilde{x}_j\right){}^j\omega_j \end{aligned} \tag{44}$$

The equations are not in the recursive form. Therefore, they are rewritten in the recursive form

$$\mathbf{Re}_{\mathrm{q_j}} = \boldsymbol{\tau}_{\mathrm{j}} - {}^j\mathbf{z}_{\mathrm{j}}^{\mathrm{T}} \times {}^j\boldsymbol{\chi}_{\mathrm{j}} - {}^j\mathbf{z}_{\mathrm{j}}^{\mathrm{T}} \times {}^j\boldsymbol{\chi}^{'}_{\mathrm{j}} \tag{45}$$

$$\mathbf{Re}_{\delta_{\mathrm{jf}}} = \mathbf{Q}_{\mathrm{jf}} - \mathbf{r}_{\mathrm{jf}}^{\mathrm{T}} \times {}^j\boldsymbol{\varphi}_{\mathrm{j}} - \boldsymbol{\theta}_{\mathrm{jf}}^{\mathrm{T}} \times {}^j\mathbf{R}_{\mathrm{j+1}}\,{}^{\mathrm{j+1}}\overrightarrow{\chi}_{\mathrm{j+1}} \tag{46}$$

$$\begin{aligned} Re_{\delta_{jf}^{'}} = & Q_{jf}^s + Q_{jf}^l - \left\{r_{jf}^{'T} \times \left({}^j\varphi_j + {}^j\varphi_j^{'}\right)\right\} \\ & - \left\{\theta_{jf}^{'T} \times {}^jR_{j+1}\left({}^{j+1}\overrightarrow{\chi}_{j+1} + {}^{j+1}\overrightarrow{\chi}_{j+1}^{'}\right)\right\} \end{aligned} \tag{47}$$

$$\mathbf{Re}_{\eta_{\mathrm{j}}} = \mathbf{F}_{\mathrm{j}} + \mathbf{Q}_{\mathrm{j}}^{'} - {}^j\mathbf{x}_{\mathrm{j}}^{\mathrm{T}} \times {}^j\overrightarrow{\boldsymbol{\varphi}}_{\mathrm{j}} \tag{48}$$

where

$$\begin{aligned} {}^j\chi_j = & {}^jT_j + {}^j\tilde{r}_{O_{j+1}/O_j}\,{}^j\varphi_j + {}^jR_{j+1}\,{}^{j+1}\chi_{j+1}\,{}^j\chi_j^{'} = {}^jT_j^{'} \\ & + {}^j\tilde{r}_{O_{j+1}/O_j}\,{}^j\varphi_j^{'} + {}^jR_{j+1}\,{}^{j+1}\chi_{j+1}^{'} \end{aligned} \tag{49}$$

$${}^j\overrightarrow{\varphi}_j = {}^jR_{j+1}\left({}^{j+1}S_{j+1} + {}^{j+1}\varphi_{j+1}\right) \quad {}^j\overrightarrow{\varphi}_j^{'} = {}^jR_{j+1}\left({}^{j+1}S_{j+1}^{'} + {}^{j+1}\varphi_{j+1}^{'}\right) \tag{50}$$

Table 4 Generalized coordinates defined for different simulation statue

$\boldsymbol{\Theta} = \left[q_1, \dot{q}_1, \delta_{11}^{'}, \dot{\delta}_{11}^{'}, \delta_{12}^{'}, \dot{\delta}_{12}^{'}, \delta_{11}, \dot{\delta}_{11}, \delta_{12}, \dot{\delta}_{12}, \eta_1, \dot{\eta}_1, q_1^m, \dot{q}_1^m\right]^T$	*F. L − F. H − F. J*
$\boldsymbol{\Theta} = \left[q_1, \dot{q}_1, \delta_{11}^{'}, \dot{\delta}_{11}^{'}, \delta_{12}^{'}, \dot{\delta}_{12}^{'}, \delta_{11}, \dot{\delta}_{11}, \delta_{12}, \dot{\delta}_{12}, \eta_1, \dot{\eta}_1\right]^T$	*F. L − F. H*
$\boldsymbol{\Theta} = \left[q_1, \dot{q}_1, \delta_{11}, \dot{\delta}_{11}, \delta_{12}, \dot{\delta}_{12}, \eta_1, \dot{\eta}_1\right]^T$	*F. L − R. H*
$\boldsymbol{\Theta} = \left[q_1, \dot{q}_1, \delta_{11}, \dot{\delta}_{11}, \delta_{12}, \dot{\delta}_{12}, \eta_1, \dot{\eta}_1, q_1^m, \dot{q}_1^m\right]^T$	*F. L − R. H − F. J*

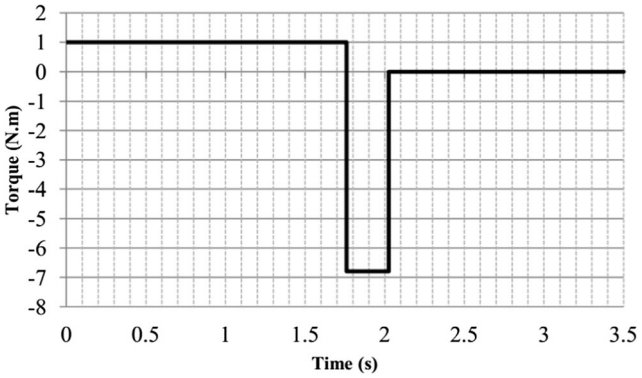

Fig. 7 Revolute joint imported torque

4 Simulation of the motion equations of FLM with flexible link and structure

To simulate the obtained dynamic equations, the system forward dynamic equation (Eq. (35)) is used. Also, the approach used to derive the final motion equations is provided in Appendix B for a single-link flexible manipulator with R-P joints. First, the mode shapes of elastic links and hubs are computed with the aid of AMM as well as Euler-Bernoulli beam theory. When calculating the deformation of elastic links, the mode shapes associated with variable link length in the clamped-free form are employed. System simulation is carried out based on the application of torque and measurement of corresponding system output (generalized coordinates). The manipulator in question consists of an elastic link with R-P joints. To simulate the system motion, four different dynamic models are utilized. The assumptions for different cases are as follows: first case—rigid hub and elastic link (*F. L − R. H*); second case—elastic hub and link (*F. L − F. H*); third case—elastic hub, link, and joint (*F. L − F. H − F. J*); fourth case—rigid hub and flexible link and joint (*F. L − R. H − F. J*). Finally, the results are compared with those of an experimental setup built in Iran University of Science and Technology, as shown in Fig. 1. For modeling the elastic deformation with good accuracy, the first two vibration modes of link and hub are used.

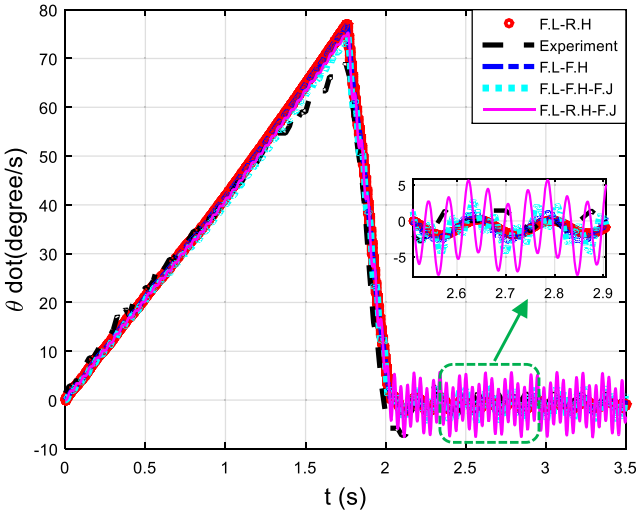

Fig. 9 Revolute joints angular velocity

Figure 5 shows a system representation composed of single-link manipulator with R-P joints. The simulation conditions are selected such that the manipulator starts motion from the rest state according to the exerted torque to the joints' motor. On this account, the torque of revolute joint remains constant during simulation, while the force of prismatic joint is applied in the form of positive and negative steps to create reciprocating motions. At the end of motion, the revolute joint is stopped using a mechanical brake, modeled as an equivalent negative torque in the simulation. The initial conditions of system simulation in four different cases are expressed according to Eqs. (51)–(54).

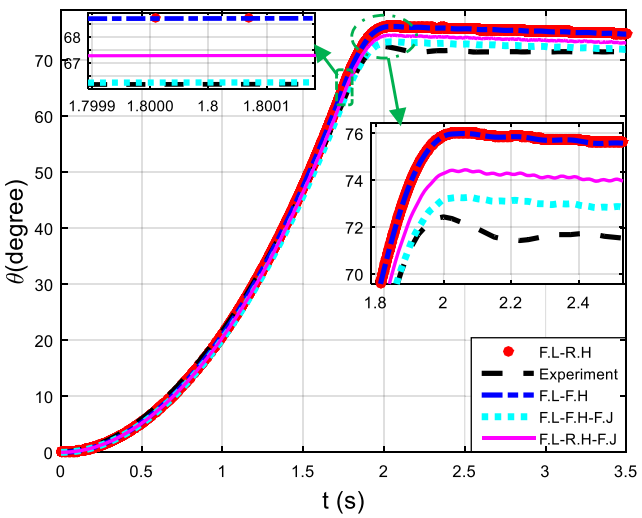

Fig. 8 Revolute joints rotational motion

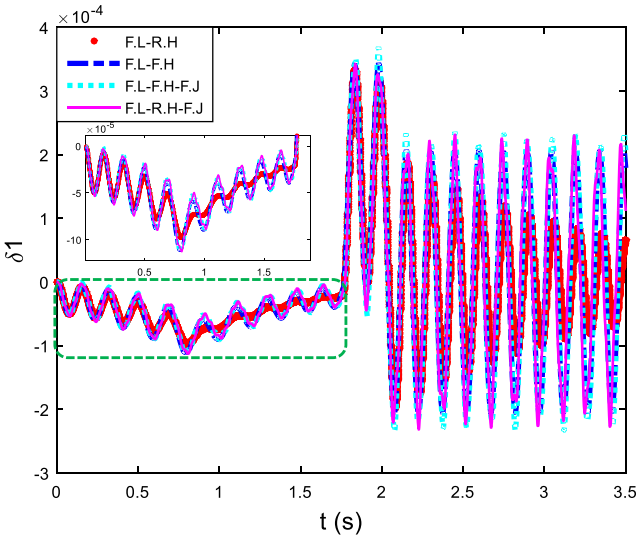

Fig. 10 First modal generalized coordinates of link

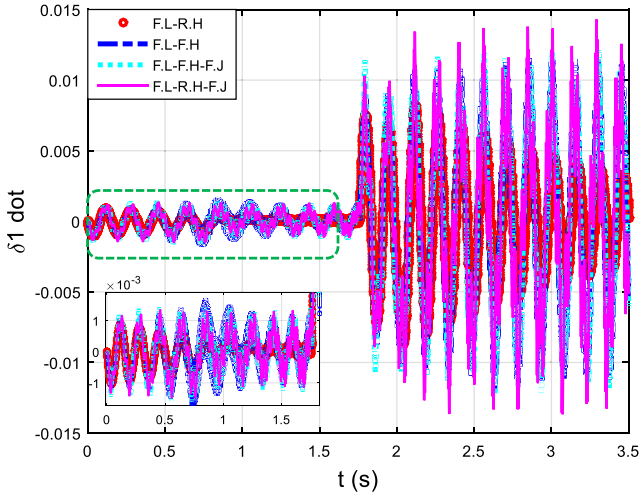

Fig. 11 Time derivatives of link's first modal generalized coordinates

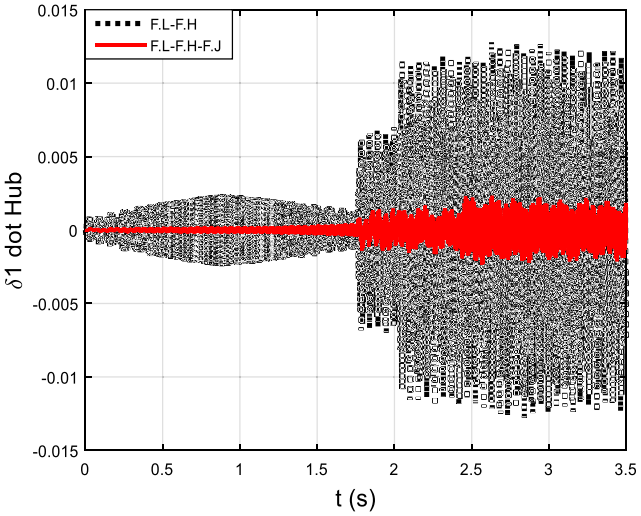

Fig. 13 Time derivatives of hub's first modal generalized coordinates

$$q_1(0) = \dot{q_1}(0) = q_1^m(0) = \dot{q}_1^m(0) = \delta_{11}(0) = \delta_{12}(0) = \dot{\delta}_{11}(0) = \dot{\delta}_{12}(0) = \delta'_{11}(0) = \delta'_{12}(0) = \dot{\delta}'_{11}(0) = \dot{\delta}'_{12}(0) = i_1(0) = 0;\ l_1(0) = 0.365 \quad for\ F.L\text{–}F.H\text{–}F.J \tag{51}$$

$$q_1(0) = \dot{q_1}(0) = \delta_{11}(0) = \delta_{12}(0) = \dot{\delta}_{11}(0) = \dot{\delta}_{12}(0) = \delta'_{11}(0) = \delta'_{12}(0) = \dot{\delta}'_{11}(0) = \dot{\delta}'_{12}(0) = i_1(0) = 0;\ l_1(0) = 0.365 for\ F.L\text{–}F.H \tag{52}$$

$$q_1(0) = \dot{q_1}(0) = \delta_{11}(0) = \delta_{12}(0) = \dot{\delta}_{11}(0) = \dot{\delta}_{12}(0) = i_1(0) = 0;\ l_1(0) = 0.365 \quad for\ F.L\text{–}R.H \tag{53}$$

$$q_1(0) = \dot{q_1}(0) = q_1^m(0) = \dot{q}_1^m(0) = \delta_{11}(0) = \delta_{12}(0) = \dot{\delta}_{11}(0) = \dot{\delta}_{12}(0) = i_1(0) = 0;\ l_1(0) = 0.365 \quad for\ F.L\text{–}R.H\text{–}F.J \tag{54}$$

By rewriting Eq. (35) for cases of interest, the coupled differential equations are formed as follows, with their difference being in the vector of generalized coordinates. Moreover, numerical methods such as Runge-Kutta are used to solve them.

$$\boldsymbol{\Theta} = \boldsymbol{\Gamma}^{-1}(\boldsymbol{\Theta}, \dot{\boldsymbol{\Theta}})\mathbf{Re} \overset{state\ \ space\ \ form}{\rightarrow} \dot{\boldsymbol{\Theta}}_1 = \boldsymbol{\Theta}_2; \dot{\boldsymbol{\Theta}}_2 = \boldsymbol{\Gamma}^{-1}(\boldsymbol{\Theta}_1, \boldsymbol{\Theta}_2)\mathbf{Re} \tag{55}$$

in which the values of generalized coordinated for three cases are determined similar to Table 4.

Figures 6 and 7 show the values of equivalent force and torque exerted to the robot's joints.

Figure 8 demonstrates the angular position of robot's revolute joint in four different simulation cases and one experimental configuration. The comparison of results shows the agreement in general trend between the rotational motion of simulated manipulator in two cases of rigid and elastic hub. However, the amount of rotation in the model with the

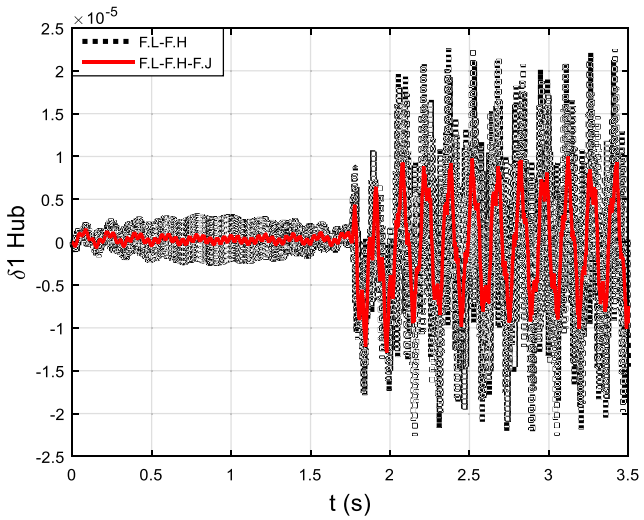

Fig. 12 First modal generalized coordinates of hub

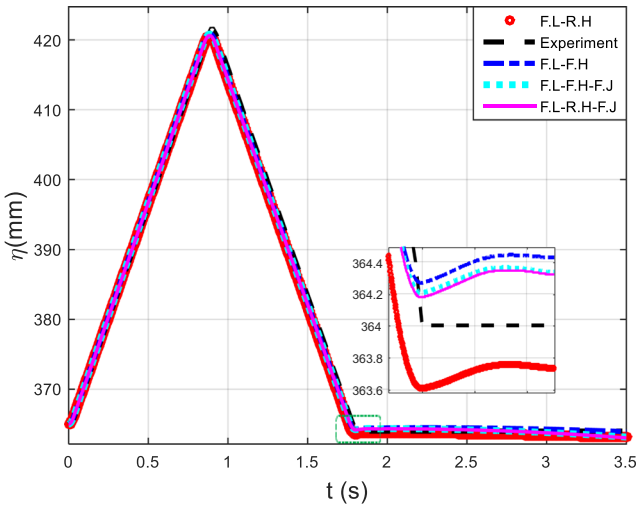

Fig. 14 Prismatic joint axial motion

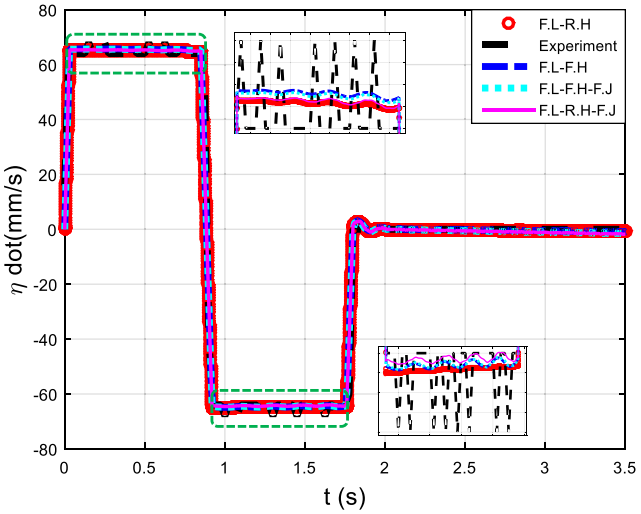

Fig. 15 Prismatic joint linear velocity

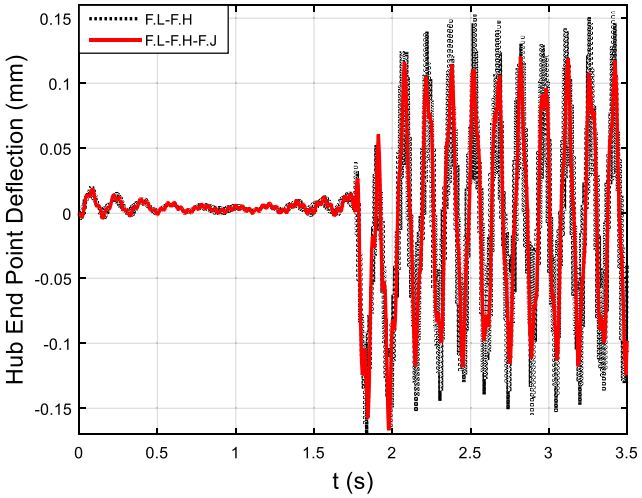

Fig. 17 Hub end-point deflection

assumption of elastic joint and hub after the simulation is closer to the results of experimental test. The reason behind the resulting difference is the mechanical brake at the end of motion in the experimental test, which causes a reverse rotation in practical implementation. By considering the magnified part of the motion in this figure, when mechanical brake and matched torques are applied, the error is minimum. However, after this point, the simulation cases and experiment slightly deviate from each other. Considering the joints' flexibility diminishes these differences.

Figure 9 shows the angular velocity of revolute joint. Based on the results, the change in the torque direction of prismatic joint influences the velocity of revolute joint, as visible at $t = 0.9$ s. Therefore, when the prismatic joint force is positive, the revolute joint velocity exceeds the modeling speed. In contrast, when the force is applied in the opposite direction, the joint velocity becomes lower than that of modeling. In addition, considering the flexibility of revolute joint's motor followed by its moment of inertia results in similarity between the presented model and the performance of actual system. Furthermore, as visible in the results, the motion of the first stage is accelerated, while it acts like a break in the second stage. Application of mechanical brake in this stage leads to negative velocity and reverse motion of the link, followed by the continuation of velocity oscillation in a way that it dampens during the course of motion. According to the stated explanations, this motion is implemented in the modeling by considering negative torque in the presented time span.

Figure 10 shows the generalized modal coordinates for the first vibration mode of manipulator's elastic link in four cases of rigid and elastic hubs as well as the assumption of joints' flexibility. In view of considering the structural damping in addition to the air damping in the rigid hub model for elastic link, vibration damping after the end of motion is attributed to the impact of Kelvin-Voigt damping coefficient. According to previous discussions, vibration amplitude rises with increasing link length and decreases with decreasing link length. Noting the considered structural vibration, after the change in the direction of applied force to prismatic joint, the

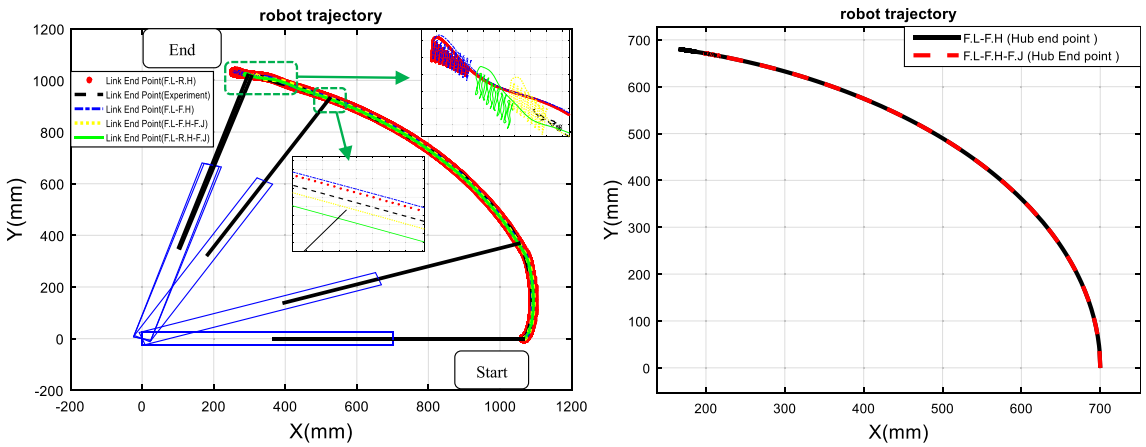

Fig. 16 Robot trajectory

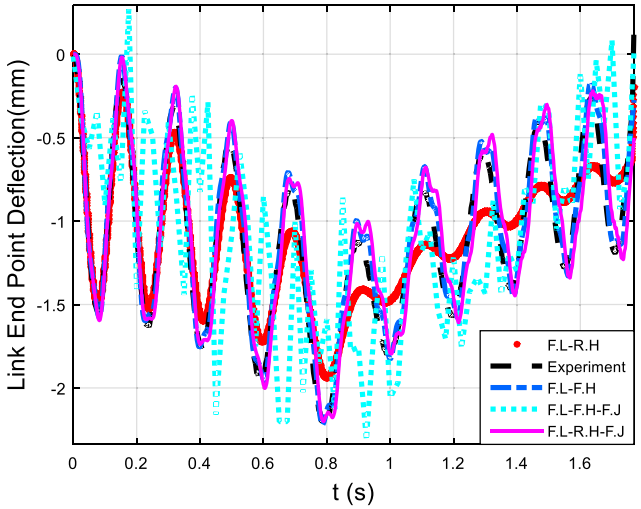

Fig. 18 Link end-point deflection

vibration amplitude rises in the case of elastic hub. However, as the structural vibration is not taken into account for the hub, the vibration amplitude decreases with the change in the force direction. In addition, after the exertion of torque at $t = 1.8$ s and application of brake, the deformation of arms is visible in the direction of brake and the vibration merely continues around the neutral axis after complete stoppage. The time derivative of generalized modal coordinates for the first mode of elastic link is displayed in Fig. 11. The link vibration amplitude prior to the change in the motion direction of prismatic joint in two cases of rigid and elastic hub is identical. However, after the change in the direction, the vibration amplitude of elastic hub increases. Moreover, the amplitude of velocity variation in a manipulator with flexible joint is more than the case in which the joints' flexibility is not considered.

Figure 12 shows the generalized modal coordinates of the elastic hub (first mode) of prismatic joint. With an increase in the elastic link length, the hub vibration amplitude increases due to the vibratory interaction between the link and joint's hub; when the link length is reduced, the oscillations' amplitude decreases. However, in view of the dimensions and material of elastic hub, the vibration amplitude of the elastic link connected to the hub is larger than hub oscillation. In addition, the vibration amplitude of the hub, unlike the link, occurs around the neutral axis. Furthermore, although considering the flexibility of revolute joint does not make a notable difference in the beam vibration, it indeed reduces the hub vibration. Accordingly, considering the joints' flexibility results in a decrease in the system structural vibration. Figure 13 shows the time derivative of the generalized modal coordinates of elastic hub. As state, when the elastic link length is increased, the hub vibration amplitude rises for the case in which the joint flexibility is not considered. However, inefficacy of these vibrations on the flexible joint state are visible.

Table 5 Mean values and standard deviations of the results

Variables	Mean value		Standard deviation	
	Experiment	F.L-F.H-F.J	Experiment	F.L-F.H-F.J
q_1	45.895	54.26	28.454	26.535
$\dot{q}_1$	20.272	17.171	18.923	24.800
η_1	378.843	373.903	23.615	16.309
$\dot{\eta}_1$	−1.702	−2.854	45.861	39.179

Figure 14 shows the longitudinal motion of flexible link inside the hub. As it can be seen, the link starts motion from the rest state and its length start to increase. After the application of reverse torque, the link motion continues in the opposite direction. The results of simulation and experimental test are in good agreement owing to the accuracy of prismatic joint and its small pitch (less than 1 mm). Figure 15 shows the linear velocity of prismatic joint. In view of the angular velocity limitation of this joint's motor in the experimental setup and, consequently, the limitation of link linear velocity, the motion of the joint is such that the link first experiences an accelerated motion so as to reach its limit velocity, after which it continues motion with constant velocity. This is also clearly visible in Fig. 7 in which upon the arrival of linear velocity to its limit value, the equivalent force is taken to be zero. Noting the application of mechanical brake after the end of motion, the generated oscillations are the consequence of this force in simulation. However, in the linear guide system related to the experimental prototype, owing to the resistive force along with the predicted mechanism used to generate linear motion, the influence of centrifugal force as a result of system rotational motion is eliminated. Consequently, as this effect is also removed from the dynamic equations, there is still a slight difference in the results, as shown in Fig. 15.

The robot trajectory consisting of the motion paths of link and hub is shown in Fig. 16. According to the presented results, the dynamic model of the single-link flexible manipulator with the assumption of elastic hub and link as well as flexible joint yields the closest response to the actual system with just 1% tolerance, although the effect of ambient conditions on system response should be considered.

Figure 17 demonstrates the elastic deformation of hub during motion. Noting the previous explanations, although the amount of hub vibration is small compared with the elastic link, its behavior affects the link motion. This is also obvious in Figs. 9 and 13.

The elastic deformation of link during motion is displayed in Fig. 18. This deformation is measured using the strain

gauges previously described. Regarding the variation visible in Fig. 18, in view of the equivalent reverse torque applied to the revolute joint to stop the system, a higher vibration amplitude compared to the actual system was observed. Furthermore, in view of the measured deformation using the strain gauges and the obtained deformation using the dynamic model, a similar trend can be observed, while the difference initiates from other ambient and structural conditions as well as measurement error. But, the maximum differences are less than the 0.1 mm. It can be stated that the accuracy for the presented model with respect to experimental results can be estimated less than 1° for revolute rotations and 1 mm for axial motions.

Table 5 represents the mean value and standard deviation of the results concluded for the case in which the joints' flexibility and the prismatic joint vibration are considered. They are also compared with the results obtained from the practical experiments conducted by the robots, presenting good agreement in practice for using this formulation in control applications.

5 Conclusion

In this article, the dynamic model of N-link flexible manipulator containing revolute-prismatic joints was presented. Compared with previous studies, taking the structural vibration of joints into account by considering the elasticity of prismatic joint's hub increased the accuracy of equations. This strategy, along with the evaluation of revolute joint flexibility as a torsional spring with a linear coefficient, helped the results become closer to real-world systems. Derivation of relations was achieved in view of time-variable equations and joints with a complex structure as well as concurrent consideration of the flexibility of hub and link aided by the recursive G-A formulation. The elastic deformation of components was found via the AMM and Euler-Bernoulli beam mode shapes. To this aim, the prismatic joint's hub was taken as an elastic link with rotational motion, while the generalized modal coordinates were distinctly defined for hub and link. The derived equations in which the interaction of structure and link was modeled were simulated for a single-link flexible manipulator in two cases of a rigid and elastic hub, followed by a comparison of results with those of empirical tests. The outputs indicated that the closest response to the experimental setup is the dynamic model of a single-link manipulator whose elasticity of link, hub, and flexible joints is considered. Thus, the differences between the linear and rotational motions of the link were found to be around 1 mm and less than 1°, respectively. In total, the difference for the system rigid-body motion was about 1 mm, while the difference was less than 1° regarding the rotary motion. In addition, the obtained results demonstrated the influence of system structural vibration on the elastic deformation due to abrupt motions such as altering the motion direction, application of an impact, and/or performing a break. A link's deflection of 2 mm was observed as a maximum link's deformation during the motion. After comparing the elastic mode results of the experimental test, it can be concluded that the reasons of differences can be looked for in ambient conditions, structure, and error of measurement method. This system can be exploited in the assembly of production lines requiring high precision, execution of industrial operations, and space, medical, and biomechanical explorations demanding high motion accuracy. For future research developments, the measurement system can be improved by using an extra measuring system such as piezoelectric materials, visions, laser scanner, accelerometer sensors, IMU sensors, and high-sensitivity lasers. The joints' dynamics is based on the concurrent use of the two models of prismatic and revolute joints as well. To this end, considering the effect of backlash, friction, damping, and flexibility are recommended, while the separate attention to mechanical brakes model in AC servo-motors is mandatory. Also, the closed-loop control algorithm can be utilized for the repetitive mission in industrial applications.

Acknowledgments The authors gratefully acknowledge the support of INSF under the grant contracts.

Appendix 1

$$\frac{\partial^{i}\omega_{i}}{\partial \ddot{q}_{j}} = {}^{i}R_{j}{}^{j}z_{j}; \frac{\partial^{i}\omega_{i}}{\partial \ddot{\delta}_{jf}} = {}^{i}R_{j}\theta_{jf}\left(L_{j}^{'}+l_{j}\right); \frac{\partial^{i}\omega_{i}}{\partial \ddot{\delta}_{jf}} = {}^{i}R_{j}\theta_{jf}^{'}\left(L_{j}^{'}\right) \tag{56}$$

$$\frac{\partial^{i}\ddot{r}_{O_i}}{\partial \ddot{q}_{j}} = {}^{i}R_{j}{}^{j}z_{j} \times {}^{i}r_{O_i/O_j}; \frac{\partial^{i}\ddot{r}_{O_i}}{\partial \ddot{\delta}_{jf}} = {}^{i}R_{j}r_{jf}\left(L_{j}^{'}+l_{j}\right) + {}^{i}R_{j}\theta_{jf}\left(L_{j}^{'}+l_{j}\right) \times {}^{i}r_{O_i/O_{j+1}} \frac{\partial^{i}\ddot{r}_{O_i}}{\partial \ddot{\delta}_{jf}} = {}^{i}R_{j}r_{jf}^{'}\left(L_{j}^{'}\right) + {}^{i}R_{j}\theta_{jf}^{'}\left(L_{j}^{'}\right) \times {}^{i}r_{O_i/O_{j+1}}; \frac{\partial^{i}\ddot{r}_{O_i}}{\partial \ddot{\eta}_{j}} = {}^{i}R_{j}{}^{i}x_{j} \tag{57}$$

Appendix 2. Motion equation derivation of R-P joints with single flexible links

In this section, the motion equations of manipulator with R-P joints are obtained for a single elastic link while the prismatic joint's hub is not considered. To this end, two different approaches are used: G-A and L-E formulations. The relative acceleration of differential element $Q$with respect to the local coordinate system $x_1y_1z_1$ can be represented as.

$$\ddot{\overrightarrow{r}}_{Q/O_1} = \begin{cases} \ddot{\eta}\,\overrightarrow{i} & \text{if} l \le \eta \le L \\ \ddot{\eta}\,\overrightarrow{i} + \ddot{\delta}(t)Y(\eta)\,\overrightarrow{j} & \text{if} L \le \eta \le L+l \end{cases} \tag{58}$$

Also, the absolute acceleration of this differential element with respect to $X_0Y_0Z_0$ (the coordinate system attached to the ground) can be represented as

$$
\begin{aligned}
{}^0\ddot{\vec{r}}_Q &= {}^1\ddot{\vec{r}}_{Q/O_1} + {}^1\dot{\vec{\omega}}_1 \times {}^1\vec{r}_{Q/O_1} + {}^1\vec{\omega}_1 \times \left({}^1\vec{\omega}_1 \times {}^1\vec{r}_{Q/O_1}\right) \\
&\quad +2{}^1\vec{\omega}_1 \times {}^1\dot{\vec{r}}_{Q/O_1} \quad {}^0\ddot{\vec{r}}_Q = \begin{cases} \left(\ddot{\eta} - \eta\dot{\theta}^2\right)\vec{i} + \left(\eta\ddot{\theta} + 2\dot{\theta}\dot{\eta}\right)\vec{j} & \text{if } l \le \eta \le L \\ \left(\ddot{\eta} - \ddot{\theta}\delta(t)Y(\eta) - \eta\dot{\theta}^2 - 2\dot{\theta}\dot{\delta}(t)Y(\eta)\right)\vec{i} + \left(\ddot{\delta}(t)Y(\eta) + \eta\ddot{\theta} - \dot{\theta}^2\delta(t)Y(\eta) + 2\dot{\theta}\dot{\eta}\right)\vec{j} & \text{if } L \le \eta \le L + l \end{cases}
\end{aligned} \tag{59}
$$

Dynamic equation based on G-A formulation

First, the system Gibbs function should be evaluated. This function is defined as

$$
\begin{aligned}
S = \; & \dot{\theta}^4 A_1 + \ddot{\theta}^2 A_1 + 4\dot{\theta}^2\dot{\eta}^2 A_2 + 4\ddot{\theta}\dot{\theta}\dot{\eta}A_3 + \ddot{\eta}^2 A_2 - 2\ddot{\eta}\dot{\theta}^2 A_3 + \delta^2(t)\ddot{\theta}^2 B_1 + \dot{\theta}^4 B_2 + 4\dot{\theta}^2\dot{\delta}^2(t)B_1 + 2\delta(t)\ddot{\theta}\dot{\theta}^2 B_3 \\
& + 4\delta(t)\ddot{\theta}\dot{\theta}\dot{\delta}(t)B_1 + 4\dot{\theta}^3\delta(t)B_3 + 2\ddot{\delta}(t)\ddot{\theta}B_3 - 2\ddot{\delta}(t)\dot{\theta}^2\delta(t)B_1 - 2\dot{\theta}^2\ddot{\eta}B_6 + 4\dot{\theta}^2\dot{\eta}^2 B_4 + \ddot{\delta}^2(t)B_1 + \ddot{\theta}^2 B_2 \\
& + \dot{\theta}^4\delta^2(t)B_1 + 4\ddot{\delta}(t)\dot{\theta}\dot{\eta}B_5 - 2\ddot{\theta}\dot{\theta}^2\delta(t)B_3 + 4\ddot{\theta}\dot{\theta}\dot{\eta}B_6 - 4\dot{\theta}^3\delta(t)\dot{\eta}B_5 + \ddot{\eta}^2 B_4 - 2\delta(t)\ddot{\theta}\ddot{\eta}B_5 - 4\dot{\theta}\dot{\delta}(t)\ddot{\eta}B_5
\end{aligned} \tag{60}
$$

where θ represents the revolute joint rotation.

$$A_1 = \int_l^L \frac{1}{2}\mu\eta^2 d\eta \tag{61}$$

$$A_2 = \int_l^L \frac{1}{2}\mu d\eta \tag{62}$$

$$A_3 = \int_l^L \frac{1}{2}\boldsymbol{\mu\eta d\eta} \tag{63}$$

$$B_1 = \int_L^{L+l} \frac{1}{2}\mu Y^2(\eta) d\eta \tag{64}$$

$$B_2 = \int_L^{L+l} \frac{1}{2}\mu\eta^2(\eta) d\eta \tag{65}$$

$$B_3 = \int_L^{L+l} \frac{1}{2}\mu\eta Y(\eta) d\eta \tag{66}$$

$$B_4 = \int_L^{L+l} \frac{1}{2}\mu d\eta \tag{67}$$

$$B_5 = \int_L^{L+l} \frac{1}{2}\mu Y(\eta) d\eta \tag{68}$$

$$B_6 = \int_L^{L+l} \frac{1}{2}\boldsymbol{\mu\eta d\eta} \tag{69}$$

Taking the derivatives of Gibbs function with respect to quasi-accelerations $\left(\ddot{\theta}, \ddot{\eta}, \ddot{\delta}\right)$ yields

$$
\begin{aligned}
\frac{\partial S}{\partial \ddot{\theta}} &= 2\ddot{\theta}A_1 + 4\dot{\theta}\dot{\eta}A_3 + 2\ddot{\theta}\delta^2(t)B_1 + 4\dot{\theta}\delta(t)\dot{\delta}(t)B_1 \\
&\quad + 2\ddot{\theta}B_2 + 4\dot{\theta}\dot{\eta}B_6 - 2\ddot{\eta}\delta(t)B_5 + 2\ddot{\delta}(t)B_3
\end{aligned} \tag{70}
$$

$$\frac{\partial S}{\partial \ddot{\eta}} = 2\ddot{\eta}A_2 + 2\ddot{\eta}B_4 - 2\dot{\theta}^2 A_3 - 2\ddot{\theta}\delta(t)B_5 - 4\dot{\delta}(t)\dot{\theta}B_5 - 2\dot{\theta}^2 B_6 \tag{71}$$

$$\frac{\partial S}{\partial \ddot{\delta}} = 2B_1\ddot{\delta}(t) + 2\ddot{\theta}B_3 + 4\dot{\theta}\dot{\eta}B_5 - 2\dot{\theta}^2\delta(t)B_1 \tag{72}$$

Now, the system potential energy will be presented. As mentioned, the link has lateral vibration in the O_1y_1 direction. Hence, the potential energy due to the elastic deformation can be represented as

$$
\begin{aligned}
V &= \frac{1}{2}\int_L^{L+l} EIy''^2 d\eta = \frac{1}{2}\int_L^{L+l} EIY''^2(\eta)\delta^2(t) d\eta \\
&= \delta^2(t)\int_L^{L+l} \frac{1}{2}EIY''^2(\eta) d\eta = \delta^2(t)C
\end{aligned} \tag{73}
$$

The conservative forces due to the elastic deformation can be represented by taking the partial derivative of potential energy with respect to quasi coordinates (θ, η, δ).

$$\frac{\partial V}{\partial \delta} = 2\delta(t)C \tag{74}$$

At this point, the system motion equation by G-A formulation can be represented as

$$\frac{\partial S}{\partial \ddot{\theta}} + \frac{\partial V}{\partial \theta} = \tau \tag{75}$$

$$\frac{\partial S}{\partial \ddot{\eta}} + \frac{\partial V}{\partial \eta} = F \tag{76}$$

$$\frac{\partial S}{\partial \ddot{\delta}} + \frac{\partial V}{\partial \delta} = 0 \tag{77}$$

Dynamic equation based on E-L formulation

First, the system kinetic energy should be evaluated. This function is defined as:

$$T = \int_l^{L+l} \frac{1}{2}\mu\left({}^0\vec{r}_Q^{\,T}\cdot{}^0\vec{r}_Q\right)d\eta = \dot{\theta}^2 A_1 + \dot{\eta}^2 A_2 + \dot{\eta}^2 B_4 + \dot{\theta}^2\delta^2(t)B_1 + \dot{\delta}^2(t)B_1 + \dot{\theta}^2 B_2 - 2\dot{\eta}\dot{\theta}\delta(t)B_5 + 2\dot{\delta}(t)\dot{\theta}B_3 \tag{78}$$

where all A and B parameters are defined in Eqs. (61–69). Next, the independent generalized coordinates are selected and substituted in E-L formulation.

$$\frac{d}{dt}\left(\frac{\partial T}{\partial \dot{\theta}}\right) - \frac{\partial T}{\partial \theta} = 2\ddot{\theta}A_1 + 4\dot{\theta}\dot{\eta}A_3 + 2\ddot{\theta}\delta^2(t)B_1 + 4\dot{\theta}\delta(t)\dot{\delta}(t)B_1 + 2\ddot{\theta}B_2 + 4\dot{\theta}\dot{\eta}B_6 - 2\ddot{\eta}\delta(t)B_5 + 2\ddot{\delta}(t)B_3 \tag{79}$$

$$\frac{d}{dt}\left(\frac{\partial T}{\partial \dot{\eta}}\right) - \frac{\partial T}{\partial \eta} = 2\ddot{\eta}A_2 + 2\ddot{\eta}B_4 - 2\dot{\theta}^2 A_3 - 2\ddot{\theta}\delta(t)B_5 - 4\dot{\delta}(t)\dot{\theta}B_5 - 2\dot{\theta}^2 B_6 \tag{80}$$

$$\frac{d}{dt}\left(\frac{\partial T}{\partial \dot{\delta}}\right) - \frac{\partial T}{\partial \delta} = 2B_1\ddot{\delta}(t) + 2\ddot{\theta}B_3 + 4\dot{\theta}\dot{\eta}B_5 - 2\dot{\theta}^2\delta(t)B_1 \tag{81}$$

For deriving Eqs. (22–24), these relations are used:

$$\dot{A}_1 = 2\dot{\eta}A_3 \tag{82}$$

$$\dot{B}_2 = 2\dot{\eta}B_6 \tag{83}$$

$$\dot{B}_3 = \dot{\eta}B_5 \tag{84}$$

$$\frac{\partial A_1}{\partial \eta} = 2A_3 \tag{85}$$

The system potential energy will be evaluated exactly similar to the previous step. Now, the system motion equation by E-L formulation can be represented as

$$\frac{d}{dt}\left(\frac{\partial T}{\partial \dot{\theta}}\right) - \frac{\partial T}{\partial \theta} + \frac{\partial V}{\partial \theta} = \tau \tag{86}$$

$$\frac{d}{dt}\left(\frac{\partial T}{\partial \dot{\eta}}\right) - \frac{\partial T}{\partial \eta} + \frac{\partial V}{\partial \eta} = F \tag{87}$$

$$\frac{d}{dt}\left(\frac{\partial T}{\partial \dot{\delta}}\right) - \frac{\partial T}{\partial \delta} + \frac{\partial V}{\partial \delta} = 0 \tag{88}$$

Comparing Eqs. (75–77) and Eqs. (86–88) shows that both approaches yield the same formulation.

Appendix 3. Computation of beam deformation using strain gauge

If the strain in different sections of an elastic beam is known, the beam shape can be estimated by interpolation. The strain of a differential element can be represented as

$$\varepsilon(x) = \frac{-t.y''}{2} \tag{89}$$

where t represents the beam thickness and y shows the link deformation. By considering the three points at which the strain gauges are placed on the links and four clamped-free boundary conditions, the beam shape can be predicted by a polynomial of sixth order as in

$$y = A.x^6 + B.x^5 + C.x^4 + D.x^3 + E.x^2 + F.x^1 + G \tag{90}$$

The equations should be solved in each step so as to find the beam shape. Due to the link length variations caused by the prismatic joints motions, the coefficient of Eq. (89) changes with respect to beam length. Therefore, two approaches can be used: (1) changing Eq. (89) to non-dimensional form and calculating the coefficients by averaging the results during the motions, and (2) computing the coefficients in each step and then finding the beam endpoint deflection. For precise and fast computation, the first approach is employed in this study. Equation (89) is changed

$$y = A.(x/l)^6 + B.(x/l)^5 + C.(x/l)^4 + D.(x/l)^3 + E.(x/l)^2 + F.(x/l)^1 + G \tag{91}$$

where l represents the length of the link located outside of the hub. The constraint equations including beam boundary conditions and deflection measurement by strain gauges leads to the following equations for evaluating the coefficients:

$$\begin{gathered} y(0) = y'(0) = 0; y''(1) = y'''(1) = 0; \\ \varepsilon(x_1/l) = \frac{-\left(30A.(x_1/l)^4 + 20B.(x_1/l)^3 + 12C.(x_1/l)^2 + 6D.(x_1/l)^1 + 2E\right)}{2} \\ \varepsilon(x_2/l) = \frac{-\left(30A.(x_2/l)^4 + 20B.(x_2/l)^3 + 12C.(x_2/l)^2 + 6D.(x_2/l)^1 + 2E\right)}{2} \\ \varepsilon(x_3/l) = \frac{-\left(30A.(x_3/l)^4 + 20B.(x_3/l)^3 + 12C.(x_3/l)^2 + 6D.(x_3/l)^1 + 2E\right)}{2} \end{gathered} \tag{92}$$

In our experimental setup, the strain gauges are attached at $x_1 = 0.125m$, $x_2 = 0.38m$, ***and*** $x_3 = 0.62m$. Using the strain

gauges recordings during the robot's motion, the coefficients are concluded, then the links deformations are evaluated using Eq. (90).

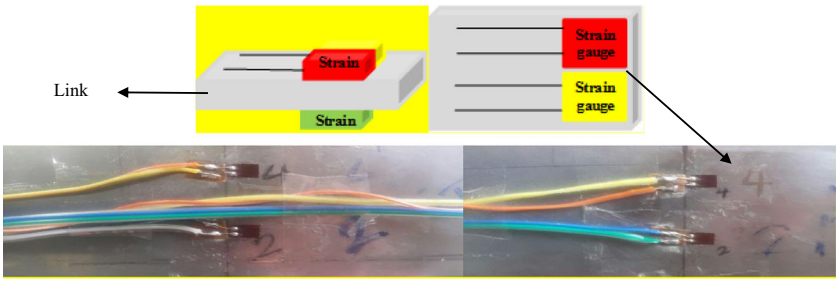

Fig. 19 Strain gauges implemented on the link

Appendix Fig. 19 represents the strain gages implemented on the link to measure the deformation in this system.

References

1. Dwivedy SK, Eberhard P (2006) Dynamic analysis of flexible manipulators, a literature review. Mech Mach Theory 41:749–777
2. Kelaiaia R (2017) Improving the pose accuracy of the Delta robot in machining operations. Int J Adv Manuf Technol 91:2205–2215
3. Lai CY, Villacis Chavez DE, Ding S (2018) Transformable parallel-serial manipulator for robotic machining. Int J Adv Manuf Technol 97:2987–2996
4. Chu M, Zhang Y, Chen G, Sun H (2015) Effects of joint controller on analytical modal analysis of rotational flexible manipulator. Chinese J Mech Eng 28:460–469
5. Bian Y, Gao Z, Lv X, Fan M (2017) Theoretical and experimental study on vibration control of flexible manipulator based on internal resonance. J Vib Control 10:463–479
6. Pedersen HC, Andersen TO, Nielsen BK (2015) Comparison of methods for modeling a hydraulic loader crane with flexible translational links. J Dyn Syst Meas Control 137:101–112
7. Walsh A, Forbes JR (2015) Modeling and control of flexible telescoping manipulators. IEEE Trans Robot 31:936–947
8. Shabana AA (1997) Dynamics of multibody systems. Multibody Syst Dyn 1:189–222
9. Book WJ (1984) Recursive Lagrangian dynamics of flexible manipulator arms. Int J Robot Res 3:87–101
10. Korayem MH, Shafei AM, Absalan F, Kadkhodaei B, Azimi A (2014) Kinematic and dynamic modeling of viscoelastic robotic manipulators using Timoshenko beam theory: theory and experiment. Int J Adv Manuf Technol 71:1005–1018
11. Lochan K, Roy BK, Subudhi B (2016) A review on two-link flexible manipulators. Annu Rev Control 42:346–367
12. Xi F, Fenton RG, Tabarrok B (1994) Coupling effects in a manipulator with both a flexible link and joint. J Dyn Syst Meas Control 116:826
13. Lu J-W, Sun X-M, Vakakis AF, Bergman LA (2015) Influence of backlash in gear reducer on dynamic of single-link manipulator arm. Robotica 33:1671–1685
14. Fenili A (2014) The rigid-flexible two link manipulator with joint friction and different number of modes for the flexible link discretization. Appl Mech Mater 706:222–232
15. Khairudin M, Mohamed Z, Husain AR, Ahmad MA (2010) Dynamic modelling and characterisation of a two-link flexible robot manipulator. J Low Freq Noise, Vib Act Control 29:207–219
16. Zhang X, Mills JK, Cleghorn WL (2009) Flexible linkage structural vibration control on a 3-PRR planar parallel manipulator: experimental results. Proc Inst Mech Eng Part I J Syst Control Eng 223:71–84
17. Bascetta L, Ferretti G, Scaglioni B (2017) Closed form Newton–Euler dynamic model of flexible manipulators. Robotica 35:1006–1030
18. Mata V, Provenzano S, Valero F, Cuadrado JI (2002) Serial-robot dynamics algorithms for moderately large numbers of joints. Mech Mach Theory 37:739–755
19. Theodore RJ, Ghosal A (1997) Modeling of flexible-link manipulators with prismatic joints. IEEE Trans Syst Man Cybern Part B 27:296–305
20. Yüksel Ş, Gürgöze M (1997) On the flexural vibrations of elastic manipulators with prismatic joints. Comput Struct 62:897–908
21. Sharifnia M, Akbarzadeh A (2016) An analytical model for vibration and control of a P R- P RP parallel robot with flexible platform and prismatic joint. J Vib Control 22:632–648
22. Al-Bedoor BO, Khulief YA (1996) Vibrational motion of an elastic beam with prismatic and revolute joints. J Sound Vib 190:195–206
23. Gordaninejad F, Azhdari A, Chalhoub NG (1991) Nonlinear dynamic modelling of a revolute-prismatic flexible composite-material robot arm. J Vib Acoust 113:461
24. Khadem SE, Pirmohammadi AA (2003) Analytical development of dynamic equations of motion for a three-dimensional flexible link manipulator with revolute and prismatic joints. IEEE Trans Syst Man Cybern Part B 33:237–249
25. Bauchau OA, Han S, Mikkola A, Matikainen MK, Gruber P (2015) Experimental validation of flexible multibody dynamics beam formulations. Multibody Syst Dyn 34:373–389
26. Korayem MH, Dehkordi SF (2017) Derivation of dynamic equation of viscoelastic manipulator with revolute–prismatic joint using recursive Gibbs–Appell formulation. Nonlinear Dyn 89:2041–2064
27. Sayahkarajy M (2018) Mode shape analysis, modal linearization, and control of an elastic two-link manipulator based on the normal modes. Appl Math Model 59:546–570
28. Celentano L, Coppola A (2011) A computationally efficient method for modeling flexible robots based on the assumed modes method. Appl Math Comput 218:4483–4493

29. Vakil M, Fotouhi R, Nikiforuk PN (2011) End-effector trajectory tracking of a flexible link manipulator using integral manifold concept. Int J Syst Sci 42:2057–2069
30. Pradhan SK, Subudhi B (2014) Nonlinear adaptive model predictive controller for a flexible manipulator: an experimental study. IEEE Trans Control Syst Technol 22:1754–1768
31. Ju J, Li W, Wang Y, Fan M, Yang X (2016) Two-time scale virtual sensor design for vibration observation of a translational flexible-link manipulator based on singular perturbation and differential games. Sensors 16:1804
32. Zhang X, Mills JK, Cleghorn WL (2007) Dynamic modeling and experimental validation of a 3-PRR parallel manipulator with flexible intermediate links. J Intell Robot Syst 50:323–340
33. Mastory CG, Chalhoub NG (2016) Nonlinear robust observer for structures with configuration-dependent natural frequencies: experimental and theoretical results. Nonlinear Dyn 85:2077–2098
34. Korayem MH, Shafei AM (2013) Application of recursive Gibbs-Appell formulation in deriving the equations of motion of N-viscoelastic robotic manipulators in 3D space using Timoshenko beam theory. Acta Astronaut 83:273–294